1 Assessing the roles emission sources and atmospheric processes play in simulating
2 $\delta^{15}N$ of atmospheric NO_x and NO_3^- using CMAQ (version 5.2.1) and SMOKE
3 (version 4.6).

5 *Huan Fang[†] and Greg Michalski[†‡]*
6
7 [†]Department of Earth, Atmospheric, and Planetary Sciences Purdue University, 550 Stadium Mall
8 Drive, West Lafayette, IN 47907, United States
9
10 [‡]Department of Chemistry, Purdue University, 560 Oval Drive, West Lafayette, IN 47907, United
11 States
12
13
14 Correspondence: Huan Fang, fang63@purdue.edu

16 Keywords: isotope, nitrogen, atmospheric NOx, atmospheric nitrate, NOx emission sources,
17 emission inventory, emission input dataset, atmospheric processes, disperse, mixing, transport,
18 chemical transport model, 3D CTM, NEI, SMOKE, CMAQ

Abstract

Nitrogen oxides (NO_x = nitric oxide (NO) + nitrogen dioxide (NO_2)) are important trace gases that affect atmospheric chemistry, air quality, and climate. Contemporary development of NO_x emissions inventories is limited by the understanding of the roles of vegetation (net NO_x source or net sink), vehicle emissions from gasoline- and diesel-powered vehicles, the application of NO_x emission control technologies, and accurate verification techniques. The nitrogen stable isotope composition ($\delta^{15}N$) of NO_x is an effective tool to evaluate the accuracy of the NO_x emission inventories, which are based on different assumptions. In this study, we traced the changes in $\delta^{15}N$ values of NO_x along the "journey" of atmospheric NO_x, driven by atmospheric processes after different sources emit NO_x to the atmosphere. The ^{15}N was incorporated into the emission input dataset, generated from the US EPA trace gas emission model SMOKE (Sparse Matrix Operator Kernel Emissions). Then the ^{15}N incorporated emission input dataset was used to run CMAQ (the Community Multiscale Air Quality Modeling System). By enhancing NO_x deposition, we simulated the expected $\delta^{15}N$ of NO_3^- assuming no isotope fractionation during chemical conversion or deposition. The simulated spatiotemporal patterns in NO_x isotopic composition for both SMOKE outputs (simulation under "emission only" scenario) and CMAQ outputs (simulations under "emission + transport + enhanced NO_x loss" scenario) were compared with corresponding measurements in West Lafayette, Indiana, USA. The simulations under "emission + transport + enhanced NO_x loss" scenario was also compared to $\delta^{15}N$ of NO_3^- in NADP (National Atmospheric Deposition Program) sites. The results indicate the potential underestimation of emissions from soil, livestock waste, off-road vehicles, and natural gas power plants and the potential overestimation of emissions from on-road vehicles and coal-fired power plants, if only considering the difference in NO_x isotopic composition for different emission sources. After considering the mixing, dispersion, transport, and deposition of NO_x emission from different sources, the estimation of atmospheric $\delta^{15}N(NO_x)$ shows better agreement (by ~3‰) with observations.

2   1. Introduction
3   Nitrogen oxides (NO_x = NO + NO_2) are important trace gases that affect atmospheric
4   chemistry, air quality, and climate. The main sources of tropospheric NO_x are anthropogenic
5   emissions from vehicles, power plants, agriculture, livestock waste, as well as natural emissions
6   from lightning and the by-product of nitrification and denitrification occurring in soil (Galloway,
7   et al., 2004). The NO_x photochemical cycle generates OH and HO_2 radicals, organic peroxy
8   radicals (RO_2), and ozone (O_3), which ultimately oxidize NO_x into NO_y (NO_y = NO_x + HONO +
9   HNO_3 + HNO_4 + N_2O_5 + other N oxides). During the photochemical processes that converts NO_x
10   to NO_y, ground-level concentrations of O_3 become elevated and secondary particles are generated
11   (Pandis and Sienfeld, 2003). Secondary aerosols that are hazardous to human health (Lighty et al.,
12   2000) and affect cloud physics, enhancing the reflection of solar radiation (Schwartz, 1996). Thus,
13   the importance of NO_x in air quality, climate, and human and environmental health makes
14   understanding the spatial and temporal variation in the sources of NO_x a vital scientific question.
15   Despite years of research, however, there are still several significant uncertainties in the NO_x
16   budget. About 15-40% of global NO_x emissions, ranging from 4 to 15 Tg N yr^{-1}, is derived from
17   global soil NO_x emissions yet evaluating and verifying emission rates using laboratory, field
18   measurements, and satellite observations is still a challenge (Jaeglé et al., 2005; Yan et al., 2005;
19   Stehfest and Bouwman, 2006; Vinken et al., 2014; Rasool et al., 2016). Soil NO_x emissions vary
20   by different biome types, meteorological conditions, N fertilizer application, and soil
21   physicochemical properties (Ludwig et al., 2001). Furthermore, the role of vegetation, acting as a
22   net source of atmospheric NO_x when ambient NO_x concentration is below the "compensation
23   point", versus acting as a net sink of atmospheric NO_x when ambient NO_x concentrations are above
24   it (Johansson, 1987; Thoene, Rennenberg & Weber, 1996; Slovik et al., 1996; Webber &
25   Rennenberg, 1996). This significantly impacts the biotic NO_x emission inventory (Almaraz et al.,
26   2018). Uncertainties also exist in the amount of NO_x emitted during the combustion of fossil fuels
27   by vehicles and industry. According to Parrish (2006), the estimation of on-road vehicle NO_x
28   emission has at least 10 to 15% uncertainty. For the mileage-based algorithm, which is used in the
29   National Emission Inventory (NEI), the uncertainty is caused by the limited number of sites to
30   determine the emission factors of vehicle classifications and emission types (Ingalls, 1989; Pierson
31   et al., 1990; Fujita et al., 1992; Pierson et al., 1996; Singer and Harley, 1996). The uncertainty in
32   power plant NO_x emissions results from the choice of emission control technologies, of which the
33   removal efficiencies of NO_x emission are different. NO_x removal by low NO_x burning, over-fire
34   air reduction, and selective non-catalytic reduction is highly variable, ranging from 50 to 75%
35   (Srivastava et al., 2005).
36   The nitrogen stable isotope composition of NO_x might be a useful tool to help resolve the
37   uncertainties of how NO_x emission sources vary in space and time because NO_x sources have
38   distinctive $^{15}N/^{14}N$ ratios (Ammann et al., 1999; Felix et al., 2012; Felix and Elliott, 2013; Fibiger
39   et al., 2014; Heaton, 1987; Hoering, 1957; Miller et al., 2017; Walters et al., 2015a, 2015b, 2018).
40   This variability in NO_x $^{15}N/^{14}N$ ratios is quantified by
41
42   $\delta^{15}NO_x$ (‰) = [($^{15}NO_x/^{14}NO_x$) / ($^{15}N_2/^{14}N_2$)$_{air}$ -1] × 1000)   Eq. (1)
43
44   where $^{15}NO_x/^{14}NO_x$ is the measurement of $^{15}N/^{14}N$ in atmospheric NO_x, compared with the ratios
45   in air N_2 = 0.0036 (For brevity, the $\delta^{15}N$ value of any NO_y compound will be denoted as $\delta^{15}NO_y$:
46   e.g. $\delta^{15}NO_3^-$). Previous research has shown that there are unique differences in $\delta^{15}N$ values for

NO$_x$ from different emission sources and significant variations within each source (Fig. 1). This uniqueness can potentially be used to partition the relative importance of various NO$_x$ sources in a mixed atmosphere. For example, Redling et al. (2003) found higher δ^{15}N of NO$_2$ in samples collected closer to the highway compared to those adjacent to a forest, showing the emissions from vehicles were dominant near the highway. A strong positive correlation between δ^{15}NO$_3^-$ and NO$_x$ emission from coal-fired power plants within 400 km radial area of study sites of deposition suggest local power plant NO$_x$ emissions impacted regional NO$_x$ budgets (Elliott et al., 2007; 2009). What is lacking is a systematic way of evaluating δ^{15}NO$_y$ values in numerous studies in the context of NO$_x$ sources, regional emissions, meteorology, and atmospheric chemistry (Elliott et al., 2009; Garten, 1992; Hall et al., 2016; Occhipinti, 2008; Russell et al., 1998).
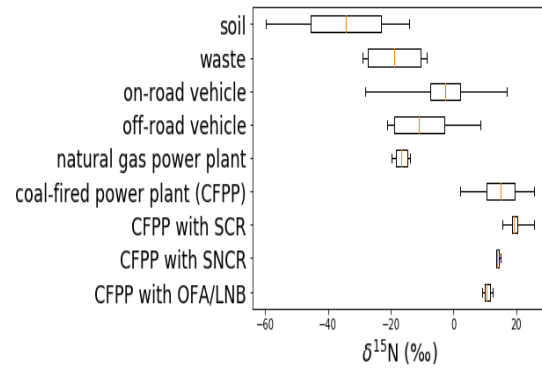
Figure 1: Box (lower quartile, median, upper quartile) and whisker (lower extreme, upper extreme) plot of the distribution of δ^{15}N values for various NO$_x$ emission sources.

Here we have simulated the emission of ^{15}NO$_x$ and its mixing in the atmosphere and compared the predicted δ^{15}N (NO$_x$, NO$_3^-$) values to observations. The δ^{15}NO$_x$ values are impacted by three main factors. The first is the inherent variability of the δ^{15}NO$_x$ emissions in time and space. Secondly, atmospheric processes that mix the emitted NO$_x$, dispersing multiple emission sources within a mixing lifetime relative to the NO$_x$ chemical lifetime (2-7 hours), which depends on its concentration and photooxidation chemistry, that also vary in time and by location (Laughner & Cohen, 2019). And thirdly, isotope effects occurring during tropospheric photochemistry may alter the δ^{15}NO$_x$ emissions as they are transformed from NO$_x$ into NO$_y$. In this paper, we consider the effects from the first and second considerations, the temporal and spatial variation in NO$_x$ emission and the impacts from atmospheric transport and deposition processes (source and mixing hypothesis). We accomplish this by incorporating an input dataset of ^{15}N emissions used in simulations by the CMAQ (Community Multiscale Air Quality) modeling system. In a previous paper we have discuss the impacts of tropospheric photochemistry by incorporating a ^{15}N chemical mechanism (Fang et al., 2021) into CMAQ. The ultimate goal is to evaluate the accuracy of the NO$_x$ emission inventory using ^{15}N.

2. Methodology
2.1 Incorporating ^{15}N into NO$_x$ emission datasets

The EPA trace pollutant emission model SMOKE (Sparse Matrix Operator Kernel Emissions) was used to simulate ^{14}NO$_x$ and ^{15}NO$_x$ emissions. ^{14}NO$_x$ emissions were estimated using the SMOKE model based on the 2002 NEI (National Emission Inventory, USEPA, 2014), and ^{15}N emissions were determined using these ^{14}NO$_x$ emissions and the corresponding δ^{15}N values of NO$_x$ sources from previous research (Table 1). Using the definition of δ^{15}N (‰), ^{15}NO$_x$ emitted by each SMOKE processing category (area, biogenic, mobile, and point) was calculated by

$$^{15}NO_x(i) = {}^{14}NO_x(i) \times {}^{15}R_{NO_x}(i) \qquad \text{Eq. (2)}$$

where $^{14}NO_x$ (i) are the NO_x emissions for each category (i) obtained from NEI and SMOKE and $^{15}R_{NOxi}$ is a ^{15}N emission factor ($^{15}NO_{xi}/^{14}NO_{xi}$) calculated by rearranging Eq. 1:

$$^{15}R_{NO_x}(i) = (\frac{\delta^{15}NO_{x(i)}}{1000} + 1) \times 0.0036 \qquad \text{Eq. (3)}$$

$\delta^{15}NO_{x(i)}$ is the $\delta^{15}N$ value of some NO_x source (i = area, biogenic, mobile, and point).

Annual NO_x emissions for 2002 were obtained from the NEI at the county-level and were converted into hourly emissions on a 12 km x 12 km grid as previously published (Spak, Holloway, & Stone, 2007). The modeling domain includes latitudes between 37 º N and 45 º N, and longitudes between 98º W and 78º W, which fully covers the Midwestern US (Fig. 2, in yellow). SMOKE categorizes NO_x emissions into four "processing categories": Biogenic, Mobile, Point, and Area (Table 1). The choice of the 2002 version of NEI is, in part, arbitrary. However, to compare the model predicted $\delta^{15}N$ values with observations, it requires the emission inventory to be relevant to the same timeframe as the $\delta^{15}N$ measurements of the NO_y. The data sets we compare to the model (discussed below) span from 2002 to 2009, thus the 2002 inventory is more relevant than later inventories (2014 onward). The county-level annual $^{14}NO_x$ emission for the Midwestern US from NEI was converted to the dataset with hourly $^{14}NO_x$ emissions.
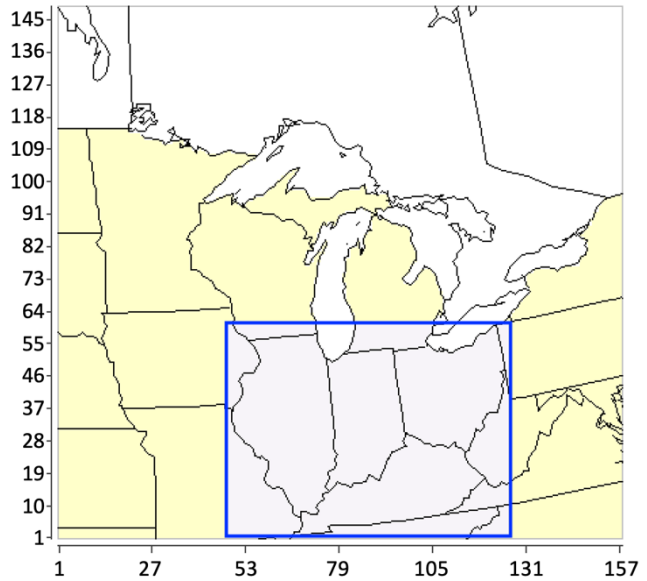
Figure 2: The full geographic domain (yellow) and extracted domain (light grayish purple) for the study.

SMOKE Category	NEI Sector	$\delta^{15}N-NO_x$ (‰) range	$\delta^{15}N-NO_x$ (‰) this study
Biogenic	Soil	-59.8 ~ -14.0	-34.3 (Felix & Elliott, 2014)
Area	Livestock Waste	-29 ~ -8.5	-18.8 (Felix & Elliott, 2014)
	Off-road Gasoline	-21.1 ~ 8.5	-11.5 (Walters et al., 2015b)
	Off-road Diesel		-10.5 (Walters et al., 2015b)
Mobile	On-road Gasoline	-28.1 ~ 17	-2.7 (Walters et al., 2015b)
	On-road Diesel		-2.5 (Walters et al., 2015b)
Point	Coal-fired Fossil Fuel Combustion	-19.7 ~ 25.6	15 (Felix et al., 2012)
	Natural Gas Fossil Fuel Combustion		-16.5 (Walters et al., 2015)
Table 1: The $\delta^{15}N$ values (in ‰) for NO_x emission sources based on SMOKE processing category and NEI sector			

2.1.1 Biogenic $^{15}NO_x$ emissions

The NO_x emission from the soil (Biogenic) was modeled in SMOKE using standard techniques (details in SA) and the $\delta^{15}N$ values of biogenic NO_x were taken from previous studies. Li & Wang (2008) measured the NO fluxes using dynamic flow chambers for 2 to 13 days after cropland soil was fertilized by either urea (n=9) or ammonium bicarbonate (n=9), and the $\delta^{15}NO_x$ ranged from -48.9‰ to -19.8‰. Felix & Elliott (2014) used passive samplers to collect NO_2 in a cornfield for 20 days, with low (-30.8‰) and high (-26.5‰) fertilizer application. Using active samplers, Miller et al. (2018) collected NO_2 between May and June finding $\delta^{15}N$ ranging from -44.2‰ to -14.0‰ (n=37); Yu & Elliott (2017) measured -59.8‰ to -23.4‰ in 15 samples from soil plots in a fallow field 2 weeks after the precipitation. Based on these studies we adopted an average $\delta^{15}N$ value for NO_x emissions from the soil of -34.3‰ (Li & Wang, 2008; Felix & Elliott, 2014; Yu & Elliott, 2017; Miller et al., 2018).

2.1.2 Mobile $^{15}NO_x$ emissions

The SMOKE NO_x emission from on-road vehicles used standard methods (details in SA) and used $\delta^{15}N$ values from prior studies. We have excluded studies that infer δ^{15} NO_x by measuring plant proxies or passive sampling in the environment (Ammann et al., 1999; Pearson et al.,2000; Savard et al. 2009; Redling et al., 2013; Felix & Elliott, 2014). This is because equilibrium and kinetic isotope effects occur as NO_x reacts in the atmosphere to form NO_y, prior to NO_x deposition. In addition, the role vegetation plays in NO_x removal and atmospheric processes that mix emitted NOx with the surroundings can also alter the $\delta^{15}NO_x$. Instead, we estimated the $\delta^{15}NO_x$ emissions from vehicles only using studies that directly measured tailpipe NO_x emissions. Moore (1977) and Heaton (1990) collected tailpipe NO_x spanning -13‰ to 2‰, with an average of -7.5±4.7‰. Neither Heaton nor Moore noted whether these 6 vehicles were equipped with any catalytic NO_x reduction technology, but it is unlikely since the late 1970 and 80's vehicles were seldomly equipped with catalytic NO_x reduction technology. Fibiger (2014) measured 5 samples of NO_x from diesel engines without SCR emitted into a smog chamber, the $\delta^{15}N$ values range from -19.2‰ to -16.7‰ (±0.97‰). The most comprehensive studies on vehicle NO_x $\delta^{15}N$ values are by Walters et al. (2015a, 2015b) who measured gas and diesel vehicles separately, including those with and without three-way catalytic converter (TCC) and SCR technology. They also measured on-road and off-road vehicles separately. The measurements showed that the $\delta^{15}NO_x$ emitted by on-road diesel vehicles ranged from -5‰ to 0‰, so the average -2.5‰ was adopted. The $\delta^{15}NO_x$ values emitted by on-road gasoline vehicles is a function of vehicle travel times, ranged from -6.3‰ to 1.8‰ with the average -2.7±0.8‰ for the Midwest region. This value is close to the measurements (-8‰ to -1‰, averaged -4.7±1.7‰) of Miller et al. (2017) who collected NO_x along highways in Pennsylvania and Ohio.

The emission rate of $^{15}NO_x$ from the mobile source was determined by Eq. 4 grid by grid, according to the contributions from on-road gasoline vehicles and on-road diesel vehicles, as well as their corresponding $\delta^{15}N$ values. NO_x emissions from off-road vehicles are regarded as area sources in SMOKE, which were processed over each county. In contrast, NO_x emissions from on-road vehicles are regarded as the mobile source in SMOKE, which will be processed along each highway. The $\delta^{15}N$ of on-road gasoline vehicles was based on the average of the vehicle travel time (t) within each region with the same zip code (Walters et al., 2015b).

$$^{15}NO_x \, (mobile) = \left(\frac{\delta^{15}NO_{x \, (on-road \, gas)}}{1000} + 1\right) \times 0.0036 \times {}^{14}NO_x \, (on-road \, gas)$$

$$+ \left(\frac{\delta^{15}NO_{x \, (on-road \, diesel)}}{1000} + 1\right) \times 0.0036 \times {}^{14}NO_x \, (on-road \, diesel) \quad \text{Eq. (4)}$$

Where $\delta^{15}NO_{x\,(on-road\,gas)} = -12.35 + 3.02 \times \ln(t + 0.455)$

2.1.3 Point source $^{15}NO_x$ emissions

NO_x point sources are large anthropogenic NO_x emitters located at a fixed position such as EGUs (electric generating units). Fugitive dust does not significantly contribute to point NO_x emissions, so our inventory focused only on power plants (Houyoux, 2005). Power plants were separated into two different types: EGU and Non-EGU (e.g. commercial and industrial combustions). The $\delta^{15}N$ value of NO_x emitted from power plants have been estimated to vary from -19.7‰ to 25.6‰ (Heaton, 1987; Heaton, 1990; Snape, 2003; Felix et al., 2012; Walters et al., 2015b). We have ignored studies that measured $\delta^{15}NO_3^-$ or $\delta^{15}HNO_3$ from EGUs (Felix et al., 2015, Savard et al., 2017) and instead, only consider those studies that directly measured $\delta^{15}NO_x$ from stacks. Heaton (1990) collected 5 samples from the different coal-fired power stations finding NO_x from 6‰ to 13‰, with a standard deviation of 2.9‰. Snape (2003) measured $\delta^{15}N$ values from power plants using three different types of coals values ranging from 2.1‰ to 7.2‰, with a standard deviation of 1.37‰ (n= 36). The most comprehensive study on coal-fired power plants NO_x values was by Felix et al. (2012). They measured the $\delta^{15}NO_x$ emission from the coal-fired power stations with and without different emission control technologies. The $\delta^{15}NO_x$ emissions range from 9‰ to 25.6‰, with the average 14.2±4.51‰ (n=42). The $\delta^{15}NO_x$ values varied when different emission control technologies were used: ranging from 15.5‰ to 25.6‰ with the average 19.4±2.28‰ (n=16) for SCR; ranging from 13.6‰ to 15.1‰ with the average 14.2±0.79‰ (n=3) for SNCR; range from 9.0‰ to 12.6‰ with the average 10.7±1.11‰ (n=15) for OFA/LNB; range from 9.6‰ to 11.7‰ with the average 10.5±0.79‰ (n=8) for no emission control technology. According to Xing et al. (2013), about half of the coal-fired power plants in the United States are equipped with SCR. Thus, we assume 15‰ for the NO_x emissions from coal-fired power plants, which is the average between SCR and other emission control technologies.

The most comprehensive study on natural gas-fired $\delta^{15}NO_x$ values (Walters et al. 2015) collected NO_x from a residential a natural gas low-NO_x furnace and the stack of a natural gas EGU. The measurement showed that the $\delta^{15}N$ values of NO_x emitted by natural gas power plants ranged that average -16.5±1.7‰, which we used for the NO_x emission from natural gas power plants. The latitude, longitude, and point sources characteristics (EGU and non-EGU, coal-fired or natural gas-fired, implementation of emission control technology) of each power plant was obtained from the US Energy Information Administration (2017). The power plants were assigned grids by their latitudes and longitudes, and the $\delta^{15}N$ values were assigned to these grids based on their emission characteristics, before determining the emission rate of $^{15}NO_x$ from point source using Eq. (2) and (3).

2.1.4 Area source $^{15}NO_x$ emissions

Area NO_x (details in SA) $\delta^{15}N$ values were based on the assumption that livestock waste and off-road vehicles (utility vehicles for agricultural and residential purposes) accounted for total area sources. Livestock waste $\delta^{15}NO_x$ values were taken from Felix & Elliott (2014) since it is currently the only study livestock waste emissions. They placed a passive sampler with ventilation fans in an open-air and closed room in barns of cows and turkeys, respectively. The $\delta^{15}NO_x$ emissions from these measurements range from -29‰ to -8.5‰. Among these samples, the $\delta^{15}NO_x$ emissions from turkey waste averaged -8.5‰, the $\delta^{15}NO_x$ emissions from cow waste averaged -24.7‰. We used -18.8‰ as the values of $\delta^{15}NO_x$ emissions from livestock waste, which is the weighted average of the from turkey waste and cow waste emissions. We used Walters et al. (2015b) to

estimate the $\delta^{15}NO_x$ emissions from the off-road vehicles since it is the latest in-depth study that measured the $\delta^{15}NO_x$ specifically from off-road vehicles that ranged from -15.6‰ to -6.2‰, averaged -11.5±2.7‰. The measurement showed that the $\delta^{15}N$ values of NO_x emitted by diesel off-road vehicles without SCR ranged from -21.1‰ to -16.8‰, averaged -19‰±2‰, and diesel-powered off-road vehicles with SCR ranged from -9‰ to 8.5‰, averaged -2‰±8‰. We adopted -10.5‰ for $\delta^{15}N$ values of NO_x emitted by diesel-powered off-road vehicle, which is the median between the measurement of vehicles with and without SCR.

The emission rate of $^{15}NO_x$ from area source was determined by Eq. 5 grid by grid, according to the contributions from waste, off-road gasoline vehicle, and off-road diesel vehicle, as well as their corresponding $\delta^{15}N$ values based on previous research.

$$^{15}NO_x \ (area) = \left(\frac{\delta^{15}NO_{x \ (waste)}}{1000} + 1\right) \times 0.0036 \times {}^{14}NO_x \ (waste)$$

$$+ \left(\frac{\delta^{15}NO_{x \ (off-road \ gas)}}{1000} + 1\right) \times 0.0036 \times {}^{14}NO_x \ (off-road \ gas)$$

$$+ \left(\frac{\delta^{15}NO_{x \ (off-road \ diesel)}}{1000} + 1\right) \times 0.0036 \times {}^{14}NO_x \ (off-road \ diesel) \quad \text{Eq. (5)}$$

The $^{15}NO_x$ emission data files of each SMOKE processing category were incorporated into the final dataset based on the $\delta^{15}N$ values from previous research (Table 1) and Eq. (2-5).

$$\delta^{15}NO_{x \ (total)} = \left(\frac{\frac{^{15}NO_x \ (area) + {}^{15}NO_x \ (biog) + {}^{15}NO_x \ (mobile) + {}^{15}NO_x \ (point)}{^{14}NO_x \ (area) + {}^{14}NO_x \ (biog) + {}^{14}NO_x \ (mobile) + {}^{14}NO_x \ (point)}}{0.0036} - 1\right) \times 1000$$

$$\text{Eq. (6)}$$

2.2 Simulating atmospheric $\delta^{15}NO_x$ in CMAQ

In order to investigate the role of mixing in the spatiotemporal distribution of $\delta^{15}NO_x$ values, CMAQ was used to simulate the meteorological transport effects (advection, eddy diffusion, etc.). In this "emission + transport" scenario, grid specific $\delta^{15}NO_x$ values emitted are dispersed as NO_x mixes across the regional scale. This dispersion will depend on grid emission strength and mixing vigor and is effectively treating NO_x as a conservative tracer. The simulations used the 2002 National Emission Inventory (NEI), as well as 2002 and 2016 meteorological conditions respectively, to explore how meteorological conditions will impact the atmospheric $\delta^{15}NO_x$. Simulations covering the full domain and extracted domain were conducted to explore and eliminate potential bias near the domain boundary.

2.2.1 Meteorology input dataset and boundary conditions

To explore the impact of atmospheric processes, the meteorology input datasets for the years 2002 and 2016 were prepared and compared. The CMAQ CTM (CCTM) used the NARR (North American Regional Reanalysis) and NAM (North American Mesoscale Forecast System) to convert the weather observations (every 3 hours for NARR, every 6 hours for NAM Analyses) into gridded meteorological elements, such as temperature, wind field, and precipitation, with the horizontal resolution of 12 km, and 34 vertical layers, with the thickness, increases with height, from 50 m near the surface to 600 m near the 50 mb pressure level. These were used to generate the gridded meteorology files on an hourly basis, using the Weather Research and Forecasting Model (WRF). To maintain consistency between the NO_x emission dataset and the meteorology,

the same coordinate system, spatial domain, and grid size used in the SMOKE model were used in the WRF simulation. The WRF outputs were used to prepare the CMAQ-ready meteorology input dataset using CMAQ's MCIP (the Meteorology-Chemistry Interface Processor; see SA for details). In these emission-only simulations, the deposition of NO_x was effectively set to zero. This was accomplished by defining $YO = {}^{14}NO$ and $YO_2 = {}^{14}NO_2$ (in addition to $ZO = {}^{15}NO$ and $ZO_2 = {}^{15}NO_2$) and setting their deposition velocities to 0.001 (setting them to zero collapses the simulation). The meteorological fields generated by MCIP were used as the inputs for Initial Conditions Processor (ICON) and Boundary Conditions Processor (BCON) to run CCTM in CMAQ. The ICON program prepares the initial chemical/isotopic concentrations in each of the 3D grid cells for use in the initial time step of the CCTM simulation. The BCON program prepares the chemical/isotopic boundary condition throughout the CCTM simulation. The CMAQ default ICON and BCON for a clean atmosphere were used, which had $NO_x < 0.25$ ppb. The ${}^{15}NO_x$ were added to the outputs of ICON and BCON, with the concentration equal to $0.0036[{}^{14}NO_x]$, which assumes $\delta^{15}N = 0$ at the initial time step and outside the domain of the simulation.

2.2.2 The role of deposition and chemical transformation of NO_x

CMAQ simulated how NO_x removal by photochemical oxidation and deposition alters $\delta^{15}NO_x$ during mixing, transport, and dispersion. This "apparent" conversion of NO_x to NO_y was implemented by enhancing NO_x dry deposition by first magnifying it to 20 times normal (14 kg/hectare/yr) and testing for the change in NO_x concentration relative to the normal deposition rate. Multiple tuning trials were conducted until the e-folding time (lifetime) of NO_x in the atmosphere across the domain averaged about 1 day. This is a typical average photochemical NO_x lifetime for a combination of urban, suburban, and rural environments (Laughner & Cohen, 2019). This approach is limited since NO_x lifetime varies depending on oxidation capacity, with urban NO_x lifetimes (~2-11 hours) being significantly shorter than in rural conditions (Fang et al., 2021). In these simulations, the molecular mass of Y and Z were set equal (14) to ensure no isotope effect was induced by dry deposition, since the equations for dry deposition have a mass term in the diffusion coefficient calculation. These "emission + transport + enhanced NO_x loss" simulations are an attempt to show how "lifetime chemistry" alters $\delta^{15}NO_x$ values by removing NO_x before it can be transported along significant distances. For example, in an "emission + transport" scenario NO_x from a high emission powerplant could travel across the domain altering regional $\delta^{15}NO_x$ as it mixes with other grids. In contrast, in the "emission + transport + enhanced NO_x loss" scenario most of that NO_x would be removed near the power plant, effectively constricting its $\delta^{15}N$ influence. This has an added advantage in that the deposited $\delta^{15}NO_x$ should be similar to the $\delta^{15}NO_3^-$, which is not being generated in this model. We emphasize that in this model the isotope effects associated with the photochemical transformation of NO_x into HNO_3 (and other higher N oxides) and deposition are ignored and will be addressed in a forthcoming paper.

2.2.4 The simulation over the extracted domain

As mentioned in section 2.2.1, atmospheric $\delta^{15}NO_x = 0‰$ for initial condition and boundary condition. As a result, a bias may occur along the boundary of the research area and mainly occurs under the following two circumstances. Firstly, when the air mass transports out of the research area (Fig. S1). Due to the lack of the emission dataset, Canada is considered an "emission-free zone" for this research. As a result, the atmospheric NO_x is diluted, which impacts its $\delta^{15}N$ values, especially for those with extreme $\delta^{15}N$ values ($\delta^{15}N < -15‰$ or $\delta^{15}N > 5‰$). Secondly, the air mass with $\delta^{15}NO_x = 0$ transports from the "emission-free zone" into the research area (Fig. S2), the
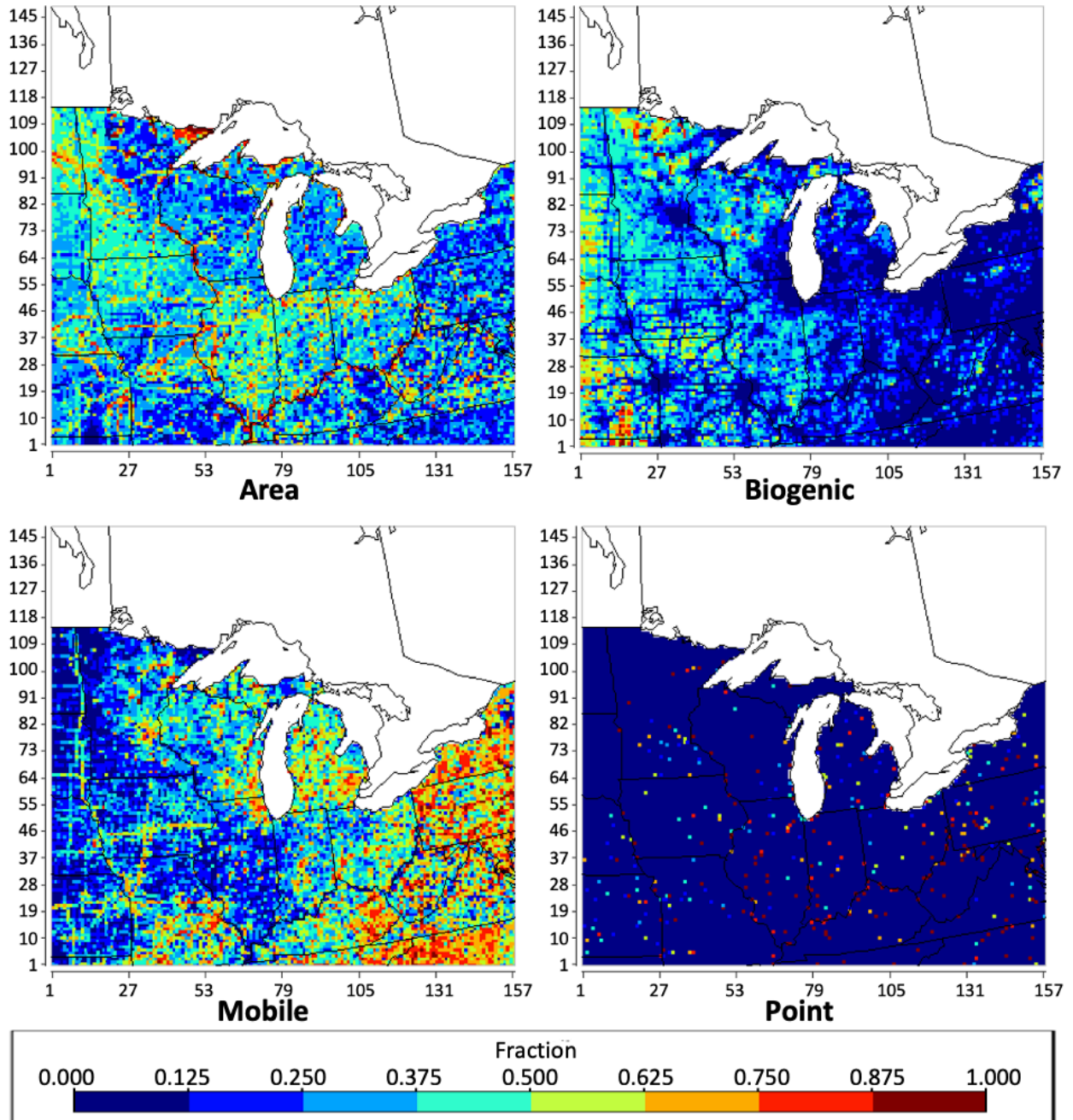
Figure 4: The geographical distribution of the fraction of NO_x emission from each SMOKE processing category (area, biogenic, mobile, point) over each grid throughout the Midwest between April and June based on NEI-2002.

atmospheric $\delta^{15}NO_x$ is flattened. Therefore, to avoid the bias near the border, the extracted domain that only covers Indiana, Illinois, Ohio, and Kentucky was determined (Fig. 2, in light purple), where the measurements of $\delta^{15}N$ values at NADP sites are available (Mase, 2010; Riha, 2013). The boundary condition for the simulation over the extracted domain is based on the CCTM output of the full-domain simulation (BCON code available on Zenodo.org (10.5281/zenodo.4311986)).

3. Results and Discussion
3.1 Simulated spatial variability of NO_x emission rates

Apr-Jun

Figure 3: Total NO_x emission in the Midwest between April and June in tons N/day. High NO_x emissions are associated with major urban areas such as Chicago, Detroit, Minneapolis-St Paul, Kansas City, St. Louis, Indianapolis, and Louisville.

We first examine the spatial heterogeneity of the NO_x emission rate for a single time period to illustrate the overall pattern of NO_x emission over the domain (Fig. 3). This is because the $\delta^{15}NO_x$ emission is determined by the fraction of each NO_x source (Eq. 6), which in turn is a function of their emission rates. Since our NO_x emissions are gridded by SMOKE using the NEI, they are, by definition, correct with respect to the NEI. However, a brief discussion of the salient geographic distribution of NO_x emissions and comparisons with other studies is warranted for completeness and as a backdrop for the discussion of NO_x fractions and resulting $\delta^{15}N$ values. We have arbitrarily chosen to sum the NO_x emissions during the April to June time period for this discussion (Fig. 3).

The April to June NO_x emissions ranged from less than 0.01 tons N/day to more than 15 tons N/day, with the seasonal grid average of 0.904 tons N/day. This average agrees well with estimates in previous studies for the United States, which were between 0.81 and 1.02 tons N/day (Dignon & Hameed, 1989; Farrell et al., 1999; Selden et al., 1999; Xing et al, 2012). Within 75% of the geographic domain, the NO_x emissions are relatively low, ranging from between 0 and 0.5 tons N/day (Fig. S3). Geographically, these grids are in rural areas some distance away from metropolitan areas and highways (Fig. 3). NO_x emissions within about 20% of the grids is relatively moderate, ranging between 0.5 and 2.0 tons N/day (Fig. S3). Geographically, these grids are mainly located along major highways and areas with medium population densities (Fig. 3). Urban centers comprise about 5% of the grids within the geographic domain and these have high NO_x emissions rates, ranging between 2.0 and 15.0 tons N/day (Fig. S3). The metropolitan area's average is 5.03 tons N/day, which is nearly 14 times of the average emission rate over the rest of the grids within the geographic domain (0.37 tons N/day) due to the high vehicle density associated with high population. The highest emissions rates are located within large cities as well as the edge of the east coast metropolitan area (Fig. 3). Summing the NO_x emissions among the grids that encompass these major midwestern cities, yields city-level NO_x emission rates that vary from 61.2 tons N/day (Louisville, KY) to 634.1 tons N/day
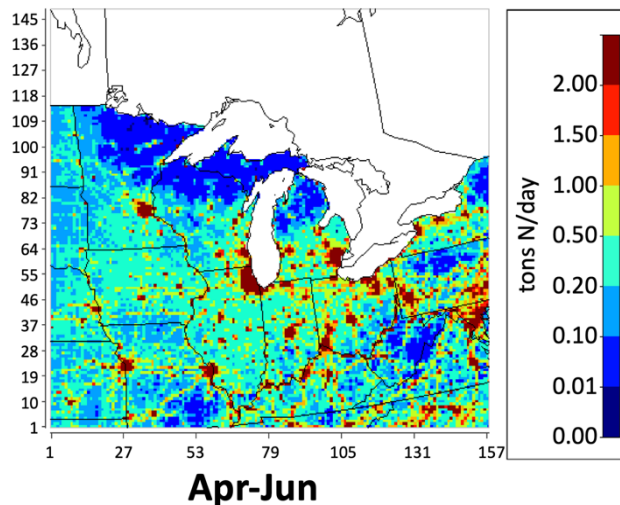
1 (Chicago, IL). These city-level NO_x emission rates (Table S4) agree well with estimates derived
2 from the Ozone Monitoring Instrument (Lu et al., 2015). Grids containing power plants are the
3 significant NO_x hotspots within the geographic domain. These account for less than 1% of the
4 grids, but the NO_x emissions from a single grid that contains a power plant can be as high as 93.4
5 tons N/day. Geographically, the power plants are mainly located along the Ohio River valley, near
6 other water bodies, and often close to metropolitan areas (Fig. 3). The NO_x emission rates of the
7 major power plants within the Midwest simulated by SMOKE (Table S5) match well with the
8 measurement from the Continuous Emission Monitoring System (CEMS) (de Foy et al., 2015;
9 Duncan et al., 2013; Kim et al., 2009). The geographic distribution of grid-level annual NO_x
10 emission density in our simulation also agrees with the county-level annual NO_x emission density
11 discussed in the 2002 NEI booklet (Fig. S4; USEPA, 2018b).
12
13   We next examine the spatial heterogeneity of the NO_x source fractions (Fig. 4) for the same
14 time period (April to June). The NO_x fraction (f) is defined as the amount of NO_x from a source
15 category (s) normalized to total NO_x (f_s =NO_x(source)/NO_x(total)). The fraction for anthropogenic
16 NO_x emission is defined as the amount of NO_x from a source category normalized to the sum of
17 NO_x emission from anthropogenic sources (f_s =NO_x(source)/(NO_x(total)-NO_x(biogenic))) Since
18 the $\delta^{15}NO_x$ is determined by the NO_x emission fractions within each grid it is important to
19 understand where in the domain these fractions differ and why. The area sources, which mainly
20 consist of off-road vehicles, agriculture production, residential combustion, as well as the
21 industrial processes, which are individually too low in magnitude to report as point sources, are
22 fairly uniform in their distribution across the domain.
23   The SMOKE simulation shows that the f_s vary significantly across the domain. The average
24 area NO_x emission fraction (f_{area}) was 0.271 for total NO_x emission and 0.290 for anthropogenic
25 NO_x emission within the Midwest from April to June. The f_{area}'s show a clear spatial variation and
26 range from 0.125 to 0.5 over about 75% of the grids (Fig. S5). Geographically, the grids with
27 relatively higher f_{area} are in the rural area away from highways, where agricultural is the most
28 common land use classification. In the states of Wisconsin and Missouri, the f_{area} is slightly lower
29 due to the higher fraction of NO_x emission from biogenic sources (f_{biog}). In the states of
30 Pennsylvania and Michigan, the f_{area} is slightly lower due to the higher fraction of NO_x emission
31 from mobile sources (f_{mobile}). In addition, the grids with f_{area} greater than 0.75 are mainly located
32 along the Mississippi River and Ohio River, due to wastewater discharge. The f_{bio} shows a clear
33 spatial variation and is highest in the western portion of the domain (Fig. 4). The f_{bio} from April to
34 June is less than 0.5 in more than 90% of the grids within the geographic domain, with the average
35 of 0.065 (Fig. S5). Geographically, the grids with relatively high f_{bio} are located in the western
36 regions of the Midwest, away from cities and highway where the density of agricultural acreage
37 and natural vegetation is high. Furthermore, the lowest f_{bio} values occur in the megacities and along
38 the highways, which agrees well with the land-use related to the biogenic emission. The April to
39 June SMOKE simulation shows that f_{mobile} of 0.325 for total NO_x emission and 0.347 for
40 anthropogenic NO_x emission. The f_{mobile} shows a clear spatial variation, with relatively higher f_{mobile}
41 are located in major metropolitan regions and along the highways, where vehicles have the highest
42 density. The value of f_{mobile} within the geographic domain distributes evenly on the histogram (Fig.
43 S5). Based on the SMOKE simulation, the fraction of NO_x emission from point sources (f_{point}) is
44 0.339 for total NO_x emission and 0.363 for anthropogenic NO_x. The f_{point}'s are obviously highest
45 in grids where the power plants are located, mainly along the Ohio River valley and near other
46 water bodies close to metropolitan areas. The point sources occupy only 4% of the domain grids

1 and about 1/4 of the power plants are not at the same grids as highways, thus these grids have a
2 f_{point} > 0.9 NO_x.
3
4 3.2   Simulated spatial variability in $\delta^{15}NO_x$
5
6
7   Using these NO_x emission source
8 fractions, the $\delta^{15}NO_x$ values were simulated
9 and the spatial heterogeneity of $\delta^{15}NO_x$ for a
10 single time period is discussed. The "emission
11 only" simulation of $\delta^{15}NO_x$ values (at 06 UTC
12 on July 26) ranged from -34.3‰ to 14.9‰
13 (Fig. 5a). The majority of the grids have
14 $\delta^{15}NO_x$ values lower than -16.3‰, which is
15 due to biogenic NO_x emissions (-34.3‰) in
16 sparsely populated areas where intensive
17 agriculture dominates the land use (Fig. 5a).
18 The $\delta^{15}NO_x$ values for grids containing big
19 cities mainly ranged between -8.75‰ and -5‰
20 due to the higher fraction of NO_x emission
21 from on-road vehicles (-2.7‰), which also
22 resolve major highways. The highest value of
23 $\delta^{15}N$ occurs at the grids, where the coal-fired
24 EGUs (+15‰) and hybrid-fired EGUs are the
25 dominant NO_x source (Fig. 5a).
26
27   The effect of atmospheric mixing on the
28 $\delta^{15}NO_x$ spatial distribution was then taken into
29 account by coupling the $^{15}NO_x$ emissions to
30 the meteorology simulation. There are
31 significant differences between $\delta^{15}NO_x$ values
32 in the "emission only" (Fig. 5a) and the
33 "emission + transport" (Fig. 5b) simulations.
34 While "emission only" $\delta^{15}N$ pattern shows
35 biogenic NO_x emissions dominating the spatial
36 domain, anthropogenic emissions become
37 dominant over most of the grids in the
38 "emission + transport" simulations, especially
39 for the grids located around major cities and
40 power plants. In general, as isotopically
41 heavier urban NO_x disperses, the grid average
42 increases from -20.2‰ under the "emission

Figure 5: The $\delta^{15}N$ values of NO_x emission, (a: "emission only" scenario) and the $\delta^{15}N$ values of atmospheric NO_x based on NEI-2002 and 2016 meteorology (b: "emission + transport" scenario), at 06 UTC on July 26, are presented by color in each grid. The warmer the color, the higher $\delta^{15}N$ values of atmospheric NO_x. The feature of the transport insides the white box is shown in Fig. 6.

43 only" scenario to -11.5‰ under the "emission + transport" scenario. Similarly, the NO_x emitted
44 along major highways is transported to the surrounding grids, so that the atmospheric NO_x at the
45 grids around the major highways becomes isotopically heavier relative to the "emission only"
46 scenario. We define $\Delta\delta^{15}N_{transport}$ as the $\delta^{15}N$ difference between "emission only" and "emission +

transport" scenarios. An example of the $\Delta\delta^{15}N_{transport}$ effect can be seen in grids encompassing a plume emanating from southern Illinois' Baldwin Energy Complex (marked with a transparent white box on Fig. 5b) that uses subbituminous coal and bituminous coal as its major energy source. The $\Delta\delta^{15}N_{transport}$ in the regions is altered as a function of distance away from the EGU. In this time snapshot (06 UTC on Jul 26), the northeastwards propagating plume of NO_x emission from the EGU creates higher $\delta^{15}NO_x$ over 135 km away (Fig. 6).
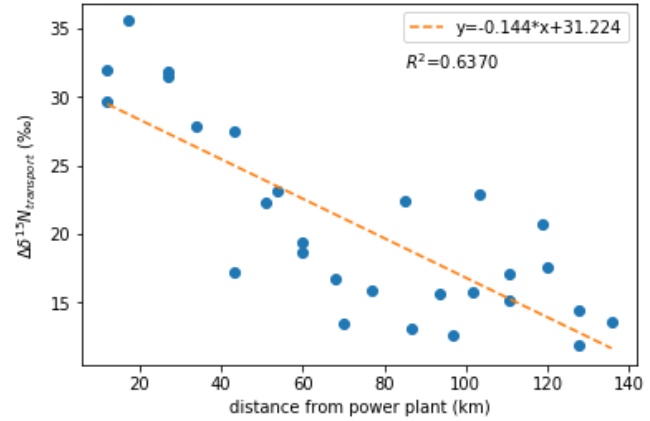
Figure 6: The $\Delta\delta^{15}N_{transport}$ along the plume (colored in dark red to orange inside the white box on Fig. 5b) over the distance from the power plant Baldwin Energy Complex (located at southwestern border of Illinois).

3.3 Seasonal variation in $\delta^{15}NO_x$

We next examine the temporal heterogeneity of $\delta^{15}NO_x$ values over the domain for "emission only" and interpret them in terms of changes in NO_x emission fractions as a function of time. The predicted $\delta^{15}NO_x$ value for total emissions in the Midwest during each season shows a significant temporal variation (Fig. 7). The $\delta^{15}NO_x$ ranged from -35‰ to 15‰, with the annual average over the Midwest at -6.15‰. The maps for different seasons show the obvious changes in $\delta^{15}N$ values over western regions of the Midwest, going from -15 to -5‰ in the spring to -35 to -15‰ in the summer. In order to qualitatively analyze the changes in $\delta^{15}NO_x$ among each season, the values over the grids (Fig. 7) were organized into the histograms (Fig. S6). The grids with $\delta^{15}NO_x$ between -35‰ and -18‰ increase dramatically from less than 10% during fall (Oct-Dec) and winter (Jan-Mar) to more than 20% during spring (Apr-Jun) and summer (Jul-Sep). The grids with $\delta^{15}NO_x$ between -18‰ and -2‰ decrease from around 90% during fall and winter to around 75% during spring and summer. The significant temporal variation in the $\delta^{15}NO_x$ during different seasons can be quantitatively explained by changing fractions of NO_x emission from the biogenic source in any grid (Fig. S7) using Eq. (6). Unlike other NO_x emission sources, the fraction of NO_x emission from biogenic sources changes significantly among each season within the geographic domain, especially over the rural areas (Fig. S7).
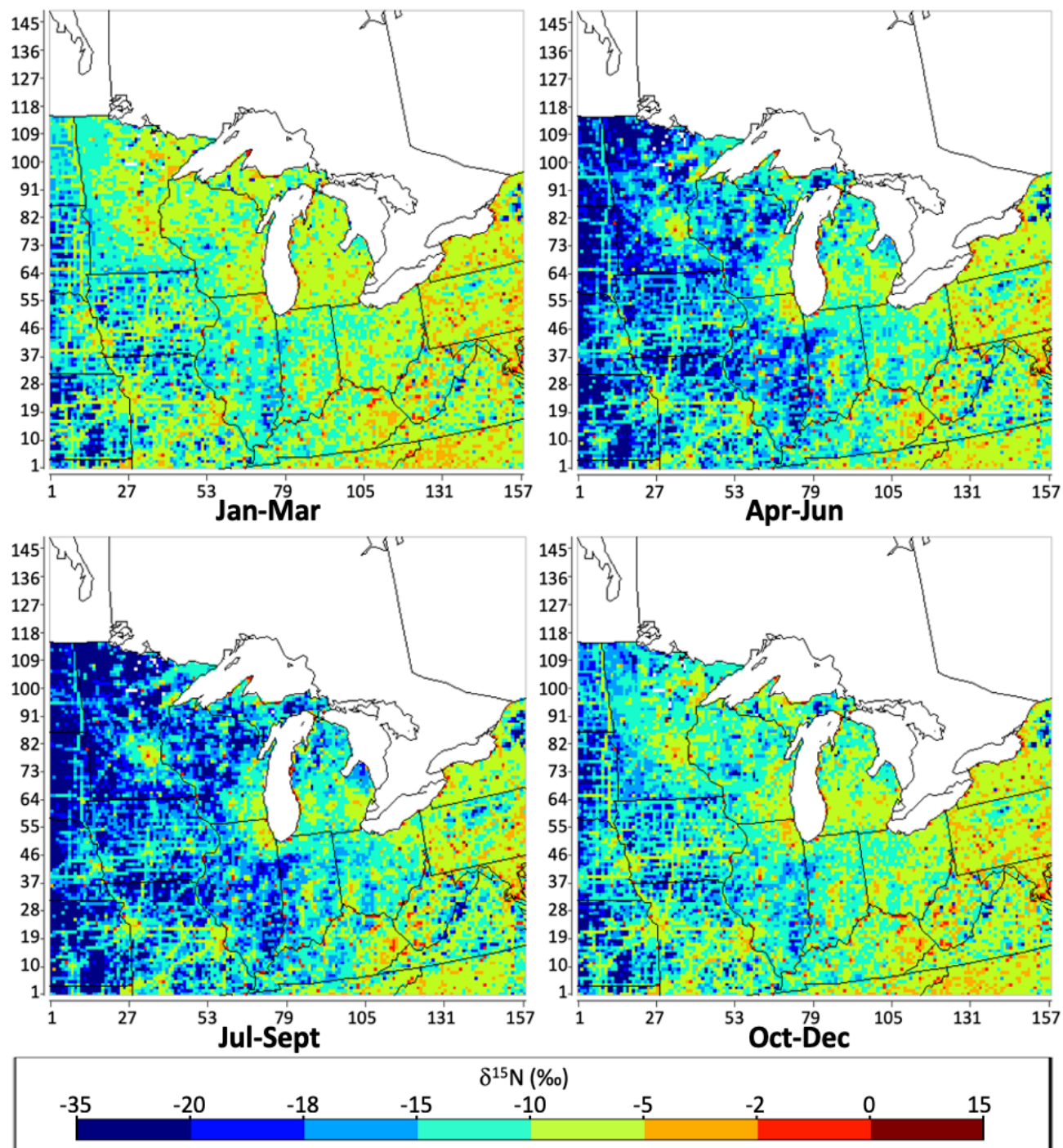
Figure 7: The geographical distribution of the $\delta^{15}N$ value of total NO_x emissions in each season (Winter: Jan-Mar; Spring: Apr-Jun; Summer: Jul-Sep; Fall: Oct-Dec) in per mil (‰) throughout the Midwest simulated by SMOKE, based on NEI-2002.

To qualitatively analyze the changes in the fraction of NO_x emission from biogenic sources among each season, the distributions of the fractions among the same cut-offs as the maps on Fig. S7 were shown in the histograms (Fig. S8). In general, the distribution of the fraction shifts to higher values during spring (Apr-Jun) and summer (Jul-Sep), indicating the increase of biogenic emissions. During this period, the surface sunlight hours, temperature, and precipitation are relatively higher and as a result, the canopy coverage of the plants becomes higher, which leads to the increase of the NO_x emission from biogenic sources (Pierce, 2001; Vukovich & Pierce, 2002; Schwede et al., 2005; Pouliot & Pierce, 2009; USEPA, 2018a). Besides this, the fertilizer application during this period is also increases soil NO_x emissions (Li & Wang, 2008; Felix & Elliott, 2014). As a result, the distribution of $\delta^{15}NO_x$ shifts to lower values during these periods (Fig. 7). The percentage of the grids with the fraction of biogenic emission less than 0.125 decreases dramatically from more than 50% during fall (Oct-Dec) and winter (Jan-Mar) to less than 35% during spring (Apr-Jun) and summer (Jul-Sep). As the NO_x emission from biogenic source becomes dominant, the percentage of the grids with $\delta^{15}NO_x$ between -35‰ and -18‰ increases, while the percentage of the grids with values between -18‰ and -2‰ decreases, which sufficiently explains the trends shown on Fig. 7.

The temporal variation in atmospheric $\delta^{15}NO_x$ is also controlled by the propagation of NO_x emissions, which varies seasonally. The temporal heterogeneity of atmospheric $\delta^{15}NO_x$ under the "emission + transport" scenario is interpreted in terms of changes in the propagation of NO_x emission as a function of time. The predicted seasonal average $\delta^{15}NO_x$ in the Midwest shows significant variations (Fig. 8). On an annual basis, the "emission + transport" average $\delta^{15}NO_x$ value was -6.10‰, which is similar to the "emission only" average range, but the range (-19.2‰ to 11.6‰) was narrower due to NO_x transport and mixing. The maps for different seasons show the obvious changes in $\delta^{15}N$ values over western regions of the Midwest, from -8.75 to -5‰ in fall and winter to -16.25 to -12.5‰ in spring and summer. The spatial heterogeneity of the $\delta^{15}NO_x$ under the "emission + transport" scenario (Fig. 8) was compared to that under the "emission only" scenario (Fig. 7). The difference was defined as $\Delta\delta^{15}N_{transport}$ (Fig. S9) and had values ranged from -21.9‰ to 31.2‰, with an average of 4.9‰. The grids with $\Delta\delta^{15}N_{transport}$ between -5‰ and 0‰ are the urban areas and decrease slightly from about 11% during fall (Oct-Dec) and winter (Jan-Mar) to 10% during spring (Apr-Jun) and summer (Jul-Sep). The grids with $\Delta\delta^{15}N_{transport}$ between 0‰ and 5‰ are typically in the rural areas that are impacted by the urban NO_x emissions and decrease dramatically from more than 50% during fall and winter to less than 40% during spring and summer. The grids with $\Delta\delta^{15}N_{transport}$ greater than 5‰, which are the rural areas obviously impacted by the urban NO_x emission and increase dramatically from less than 40% during fall and winter to more than 50% during spring and summer. Therefore, the impacts from transport and mixing are more obvious during spring and summer (Fig. S10).
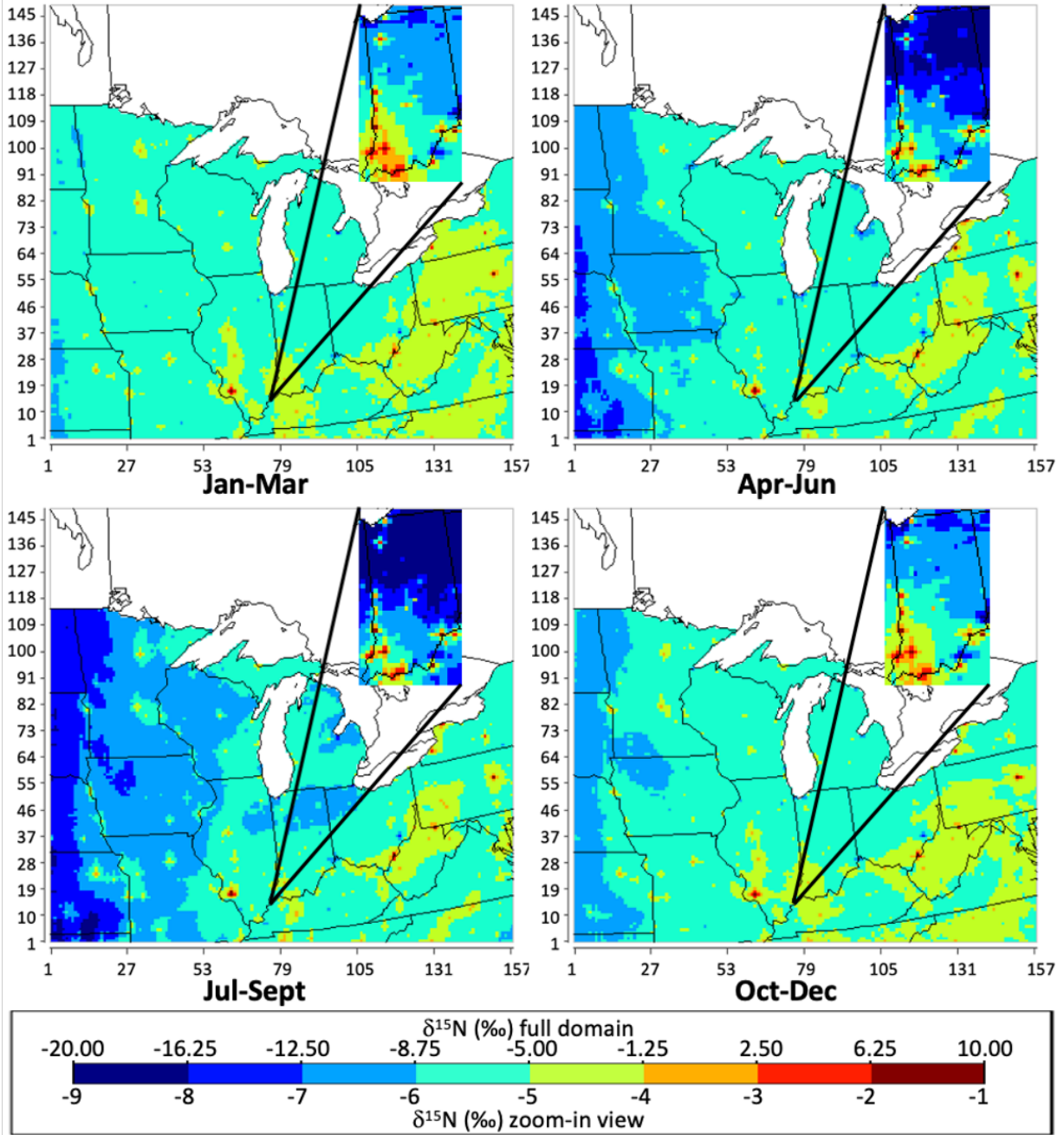
Figure 8: The geographical distribution of the $\delta^{15}N$ value of atmospheric NO_x in each season (Winter: Jan-Mar; Spring: Apr-Jun; Summer: Jul-Sep; Fall: Oct-Dec) in per mil (‰) throughout the Midwest (with zoom-in view focusing on Indiana) simulated by CMAQ, based on NEI-2002 and 2016 meteorology.

The PBL height is an effective indicator showing whether the pollutants are under synoptic conditions, which are favorable for the dispersion, mixing, and transport after being emitted into the atmosphere (Oke, 2002; Shu et al., 2017; Liao et al., 2018; Miao et al., 2019). Comparing the distributions $\Delta\delta^{15}N_{transport}$ values (Fig. S9) with the corresponding PBL height (Fig. S11) for each season, the effects of PBL height on the propagation of the air mass are clearly shown. NO_x emitted by power plants is much higher than the emission rates at the surrounding grids and is a hotspot that impacting the $\delta^{15}N$ values at the surrounding grids. As PBL increases, the emitted NO_x from power plant mixes more effectively with the surrounding grid, thus there are higher $\delta^{15}NO_x$ values along the power plant plume transect. The PBL height changes significantly among each season within the geographic domain, especially over Minnesota, Wisconsin, and Iowa (Fig. S11). The PBL height over these areas increases from less than 250 meters above the ground level to more than 625 meters above the ground level, during spring and summer, which creates a more favorable synoptic condition for the dispersion, mixing, and transport of the pollutants after being emitted into the atmosphere. As a result, the difference in $\delta^{15}N$ values shifts to higher values, showing the stronger effect of atmospheric processes during spring and summer. In order to qualitatively analyze how PBL height affects the $\delta^{15}NO_x$ along power plant plumes, the domain average PBL height for each month was plotted against $\delta^{15}NO_x$ (Fig. 9a). The $\delta^{15}N$ values along the power plants plumes and PBL heights over the domain have the same seasonal trend. Interestingly, the "turning point" of the $\delta^{15}N$ values is about one month later than the "turning point" of the PBL heights. The scatter plot (Fig. 9b) shows a strong positive correlation (R^2=0.85) between the domain average PBL height and average $\delta^{15}N$ value along the power plants plumes. The positive correlation between PBL height and propagation of air mass, indicated by the evolution of atmospheric $\delta^{15}NO_x$ in this study, agrees well with the corresponding measurement in megacities in China from the previous studies (Shu et al., 2017; Liu et al., 2018; Liao et al., 2018.
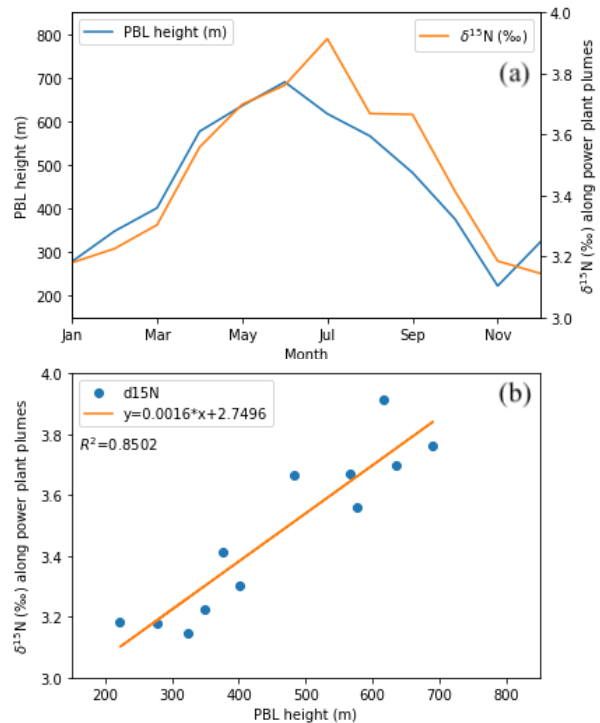
Figure 9: The time series plot (a) and the scatter plot (b) of the domain average PBL height (m) and the average $\delta^{15}N$ (‰) value of atmospheric NO_x along the plumes of power plants during each month throughout the Midwest simulated by CMAQ, based on NEI-2002 and 2016 meteorology.

3.4 The simulations based on different meteorology input datasets

The spatial heterogeneity of the $\delta^{15}NO_x$ using 2016 meteorology input dataset was compared to that using 2002 meteorology (Fig. S13). Overall, the simulated $\delta^{15}NO_x$ using 2002 meteorology has the similar geographic distribution and seasonal trend as the 2016 simulation. The difference was defined as $\Delta\delta^{15}N_{2002-2016}$ (Fig. 10) and had values ranged between -1.25‰ and +1.25‰ over most of the grids. However, in the western part of the domain, where the biogenic NO_x emission
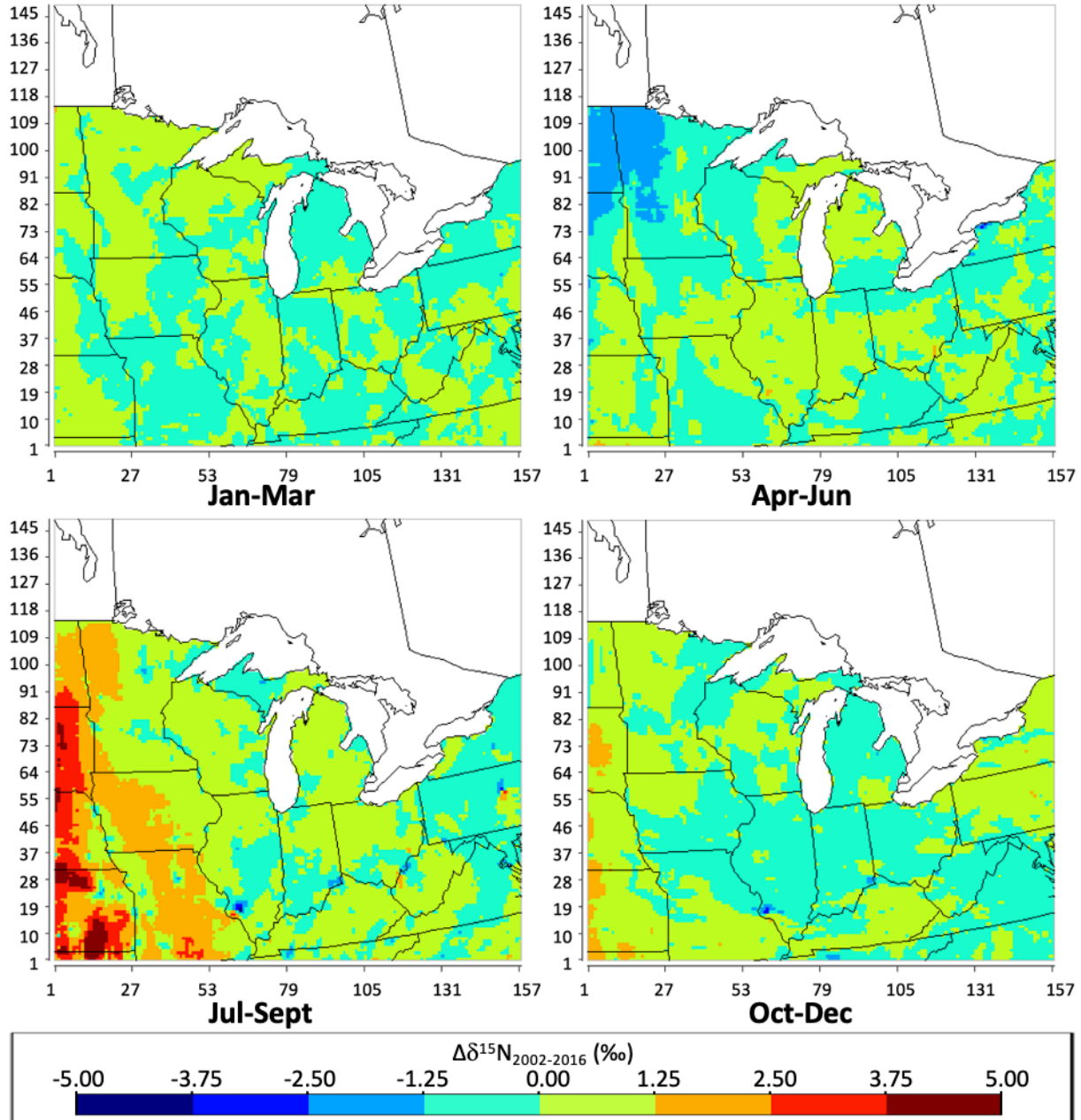
Figure 10: The difference between the $\delta^{15}N$ (‰) value of atmospheric NO_x based on 2016 meteorology and 2002 meteorology ($\Delta\delta^{15}N_{2002-2016}$) during each season (Winter: Jan-Mar; Spring: Apr-Jun; Summer: Jul-Sep; Fall: Oct-Dec), throughout the Midwest simulated by CMAQ.

is dominant, the more positive $\Delta\delta^{15}N_{2002\text{-}2016}$ values (up to 5‰) during summer and fall occur. On the other hand, the more negative $\Delta\delta^{15}N_{2002\text{-}2016}$ values (up to -5‰) occur along the power plant plume during the same period. The spatial heterogeneity of $\Delta\delta^{15}N_{2002\text{-}2016}$ indicates how climate change alters the $\delta^{15}NO_x$. If we have enough input datasets to generate and compare the seasonal/monthly $\delta^{15}NO_x$ over the past 20+ years, the impacts of anomalies in each meteorology variables could be explored. For the current dataset, the similar comparison between the $\delta^{15}NO_x$ and the corresponding PBL height was conducted for the simulation based on 2002 meteorology (Fig. S14) to show how PBL height changes the evolution of $\delta^{15}NO_x$. Under the 2002 meteorology, lower PBL height during the winter caused surface $\delta^{15}NO_x$ values along the power plants' plumes to be lower relative to 2016 meteorology. On the other hand, due to the higher PBL height during the 2002 spring and summer the $\delta^{15}N$ values decreased through July before ending with the relatively higher $\delta^{15}N$ values in December. The scatter plot for the simulation based on 2002 meteorology (Fig. S14b) also shows a strong positive correlation between the domain average PBL height and average $\delta^{15}N$ value along the power plants plumes, with R^2=0.78. The videos of atmospheric $\delta^{15}NO_x$ on an hourly basis throughout the years 2002 and 2016 are available on Zenodo.org (10.5281/zenodo.4311986).

3.5 The simulation over the extracted domain

Analysis of the whether there was difference between the extracted-domain simulation (Fig. 2) and full-domain simulation was conducted by defining $\Delta\delta^{15}N_{extracted\text{-}full}$ and assessing the bias due to the motion of the air mass across the domain boundary (Fig. S17). The $\Delta\delta^{15}N_{extracted\text{-}full}$ values ranged between -0.25‰ and +0.25‰ over most of the grids, showing the difference between extracted-domain simulation and full-domain simulation of $\delta^{15}N$ values are usually trivial. However, near the southern border of the extracted domain $\Delta\delta^{15}N_{extracted\text{-}full}$ values close to +0.75‰ (fall and winter) and close to +1.00‰ (spring and summer) suggesting extracted domain may be required for accurate $\delta^{15}NO_x$ simulations

3.6 The role of enhanced NO$_x$ loss

The "emission + transport + enhanced NO$_x$ loss" simulations significantly alter the $\delta^{15}NO_x$ relative to the "normal deposition" scenarios. Again, the enhanced NO$_x$ loss cases are removing NO$_x$ at rates similar to those by removal via its conversion into HNO$_3$. Thus, the NO$_x$ deposited is ~ $\delta^{15}NO_3^-$ (assuming no photochemical isotope effects) and the $\delta^{15}NO_x$ is that in the residual NO$_x$. The impact of enhanced NO$_x$ loss on the residual NO$_x$ was assessed using $\Delta\delta^{15}N_{hi\text{-}no}$, the difference between the $\delta^{15}NO_x$ values under the "enhanced NO$_x$ loss" and "no deposition" scenarios. The $\Delta\delta^{15}N_{hi\text{-}no}$ range was ±4‰ and was especially obvious downwind of the locations with large emission rates, such as power plants or megacities (Fig. 11). This can be explained in a similar

Jul 25 18 UTC
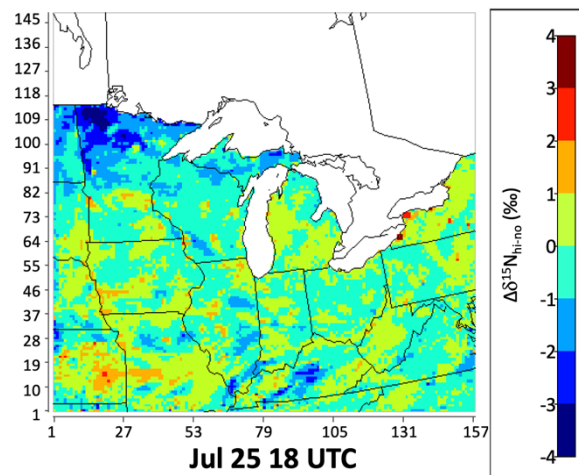
Figure 11. The $\Delta\delta^{15}N_{hi\text{-}no}$ values at 18 UTC on July 25.

1   fashion to the "no deposition" scenarios (Fig. S18a), where the dispersion of the isotopically
2   heavier NO_x emission from big cities, major highways, and power plants elevated the $\delta^{15}NO_x$
3   values in rural areas and the dispersion of the isotopically lighter biogenic NO_x emission lowered
4   the $\delta^{15}NO_x$ values in the surrounding grids located in the suburb of major cities (Fig. S18b). When
5   "enhanced NO_x loss" is used the transport, mixing, and dispersion of local NO_x emissions are
6   restricted to smaller geographical extent (Fig. S18b) leading to different $\delta^{15}NO_x$ values relative to
7   no deposition. The temporal heterogeneity of $\Delta\delta^{15}N_{hi-no}$ over the domain was examined and the
8   impact of enhancing deposition rates of NO_x on the $\delta^{15}N$ of atmospheric NO_x on a seasonal basis
9   was explored (Fig. 12). The seasonal $\Delta\delta^{15}N_{hi-no}$ values range from -3.67‰ to 5.34‰, with an
10   average of 0.51‰. The overall pattern of the $\Delta\delta^{15}N_{hi-no}$ values shows that due to deposition, the
11   atmospheric NO_x became isotopically lighter over the majority of the grids since EGU and vehicle
12   NO_x is not being transported as far. Conversely, in grids that contain or surround power plants and
13   big cities the $\delta^{15}NO_x$ increases because it is not as effectively mixing with low $\delta^{15}NO_x$ from nearby
14   grids. The enhanced NO_x loss simulation was used as a proxy to present the isotope effects
15   associated with the "pseudo photochemical transformation" of NO_x into NO_y. The complete
16   isotope effect of tropospheric photochemistry will be addressed in future work, which incorporates
17   ^{15}N into the chemical mechanism of CMAQ for the simulation.
18   The $\delta^{15}NO_x$ value of dry deposition (a proxy for $\delta^{15}NO_3^-$) simulated by CMAQ show similar
19   monthly variations and seasonal trends as SMOKE (Fig. S22). The ranges of $\delta^{15}NO_x$ values within
20   each month were narrower, compared to the simulation from SMOKE, with a minimum during
21   February (-8.7~ -4.4‰) and a maximum during August (-11.8~-4.2‰). The seasonal trend shows
22   low $\delta^{15}NO_x$ values in deposition during summer, with the median around -7.4‰, and slightly
23   higher values during winter (median around -6.0‰). Therefore, the CMAQ simulation inherits the
24   monthly variations and seasonal trends from SMOKE, while the atmospheric NO_x becomes
25   isotopically heavier, after taking atmospheric mixing and transport into account. As mentioned
26   above, most of the NADP sites are located away from big cities and power plants. Thus, the
27   atmospheric mixing and transport led to the isotopically heavier atmospheric NO_x.
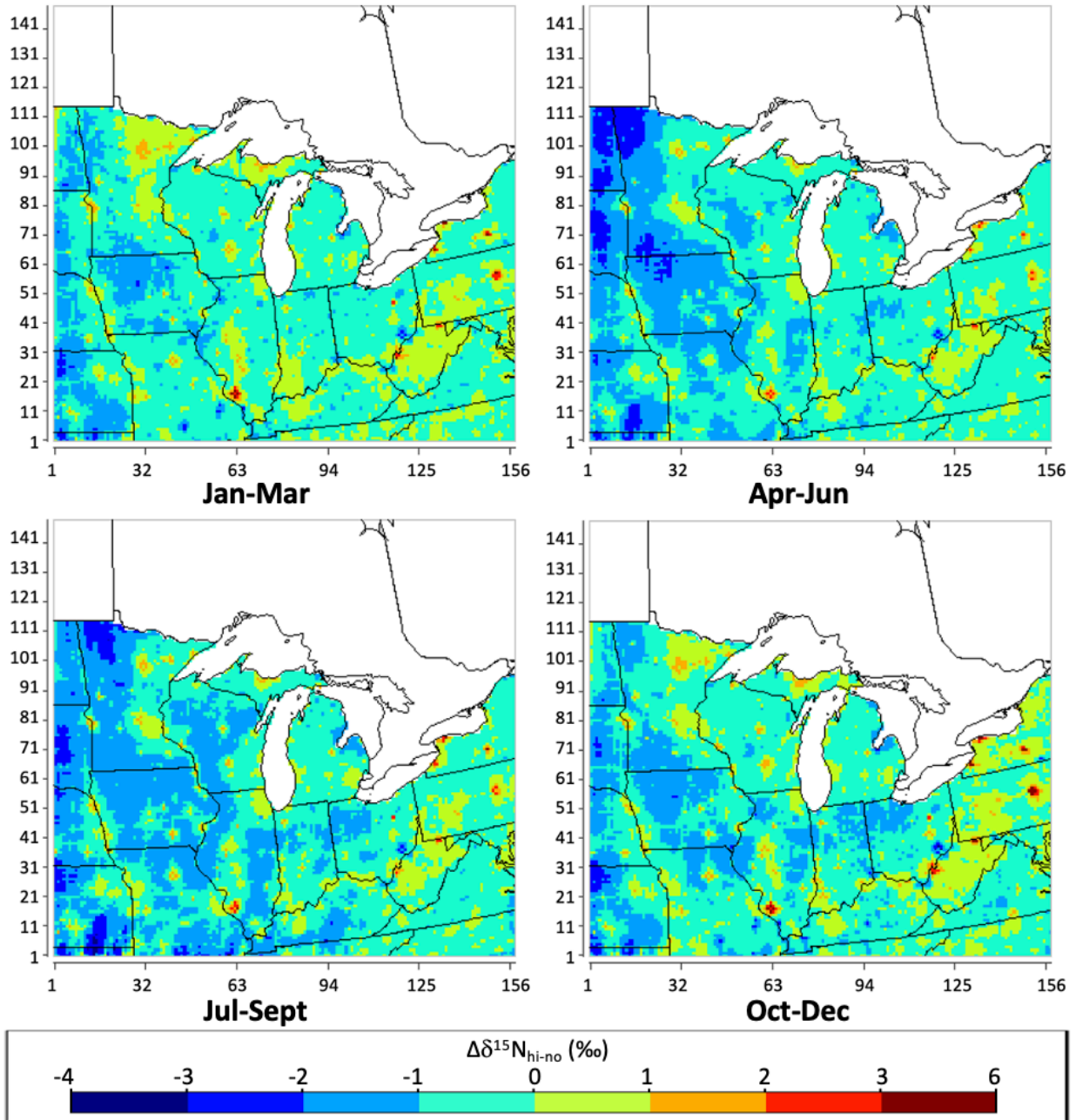
Figure 12: The difference between the $\delta^{15}N$ (‰) value of atmospheric NO_x under the "enhanced NO_x loss" scenario and "no deposition" scenario ($\Delta\delta^{15}N_{hi-no}$) during each season (Winter: Jan-Mar; Spring: Apr-Jun; Summer: Jul-Sep; Fall: Oct-Dec), throughout the Midwest simulated by CMAQ, based on NEI-2002 and 2016 meteorology.

2
3
4
5
6

3.7   Model-observation comparison of $\delta^{15}NO_x$

In order to evaluate the SMOKE/CMAQ simulations of atmospheric $\delta^{15}NO_x$, they were compared to two recent studies of $\delta^{15}NO_x$. The first comparison was relative to rainwater measurements in West Lafayette, IN from July 9 to August 5, 2016 (Walters, Fang, & Michalski, 2018). The measured $\delta^{15}NO_x$ values ranged from -33.8‰ to 0.2‰, with the median of -11.2±8.02‰. Under the "emission + transport + enhanced NO_x loss" scenario using 2016 meteorology, the simulated $\delta^{15}NO_x$ mean (-7.9±2.19‰) was 3.3‰ less negative than the observations and the range (-15.9‰ to -3.7‰) was about half that in the observations (Fig. 13, top, Table S7). The predicted $\delta^{15}NO_x$ was similar regardless of whether 2016 or 2002 meteorology was used but were closer to the measured values, comparing to the "emission only" simulations (Fig. 13, top). It is not surprising that the measurements are more negative than the observations because the model does not account for isotope fractionation during the conversion NO_x into NO_y. Our previous work has shown the photochemical isotope effect enriches NO_y and depletes NO_x (Fang et al., 2021; Walters and Michalski, 2015) and thus the lower measured $\delta^{15}NO_x$ relative to model is consistent with this isotopic depletion.

Figure 13: The $\delta^{15}NO_x$ distributions at Lafayette, IN (top) and along Midwest highways (bottom), simulated by SMOKE (a), CMAQ based on 2016 (b) and 2002 meteorology (c), compare with the measured $\delta^{15}NO_x$ (d) (box: lower quartile, median, upper quartile; whisker: lower extreme, upper extreme)

Our model simulations were also compared to on-road vehicle plume measurement along Midwest highways from August 8 to 18, 2015 (Miller et al., 2017). The boxplot also shows more accurate estimation of $\delta^{15}N$ after considering the atmospheric mixing with the emission from surrounding grids (Fig. 13, bottom). Using the "emission only" scenario, the simulated $\delta^{15}NO_x$ mean was about 3‰ more negative than the observations. The predicted $\delta^{15}NO_x$ under the "emission + transport + enhanced NO_x loss" scenario for these samples along Midwest highways was closer to the measured values, compared to the "emission only" simulations, using no matter 2016 or 2002 meteorology. The modeled values are quite close to the observations suggesting the photochemical isotope effect is small for these samples. This is not surprising given they were collected on major

highways where NO_x concentrations are high and the timescale between collection and emission
is small and thus only a small fraction of emitted NO_x would have been converted to NO_y
minimizing the photochemical isotope effect.

The 30 fold enhanced NO_x loss (see methods) was used to simulate the $\delta^{15}N$ value of NO_3^-
deposition ($\delta^{15}NO_3^-$) that was then compared to observations (Fig. 14). As previously noted, rather
than explicitly converting NO_x into NO_y via the chemical mechanism in CMAQ, which would
require writing an isotope-enabled chemical scheme with appropriate rate constants, we amplified
NO_x deposition as a surrogate. This amplification reduced the NO_x lifetime to about 1 day, thus
by calculating the $\delta^{15}NO_x$ in the deposition fraction, as opposed to residual NO_x in the atmosphere,
we are approximating the $\delta^{15}NO_3^-$ in deposition. The simulated $\delta^{15}NO_3^-$ was compared to NO_3^-
collected at NADP sites within Indiana, Illinois, and Ohio in the year 2002 (Table S4). The NEI-2002 and WRF2002 were used for the SMOKE emission model and CMAQ simulations,
respectively. The value in deposition was calculated by $\delta^{15}NO_3^- = \Sigma f_{NOxhr} \delta^{15}NO_{xhr}$, where f_{NOxhr}
is the hourly mole fraction of NO_x isotopologue deposited ($f_{NOxhr} = NO_{xhr}/NO_{xT}$) and $\delta^{15}NO_{xhr}$ is
the $\delta^{15}N$ value of NO_x in deposition. The total NO_x deposited (NO_{xT}) used to calculate f_{NOxhr} was
the amount deposited 5 days prior to the sampling date since the NADP deposition collection
integrate the week.

The $\delta^{15}N$ values of NO_x deposition simulated by CMAQ under the "emission + transport + enhanced NO_x loss" scenario at each site were compared with the measurements of $\delta^{15}N$ values of NO_3 from prior studies (Mase, 2010; Riha, 2013). While the scatter plot shows a moderate positive correlation between observed and simulated $\delta^{15}NO_3^-$, the simulated value is consistently lighter than the sample $\delta^{15}NO_3^-$ (Fig. 14, top). The magnitude of this negative bias varies among the NADP sites (Fig. S23) and is attributed to isotope fractionation during the conversion NO_x into NO_y, which enriches NO_3^- (Fang et al., 2021; Walters and Michalski, 2015). Globally this enrichment has been estimated at 3.9±1.8‰ (Song et al, 2021). But this enrichment is a function of NO_x, VOC, and oxidant loading, as well as temperature, and photolysis rate (Fang et al., 2021) and is not expected to be the same at each
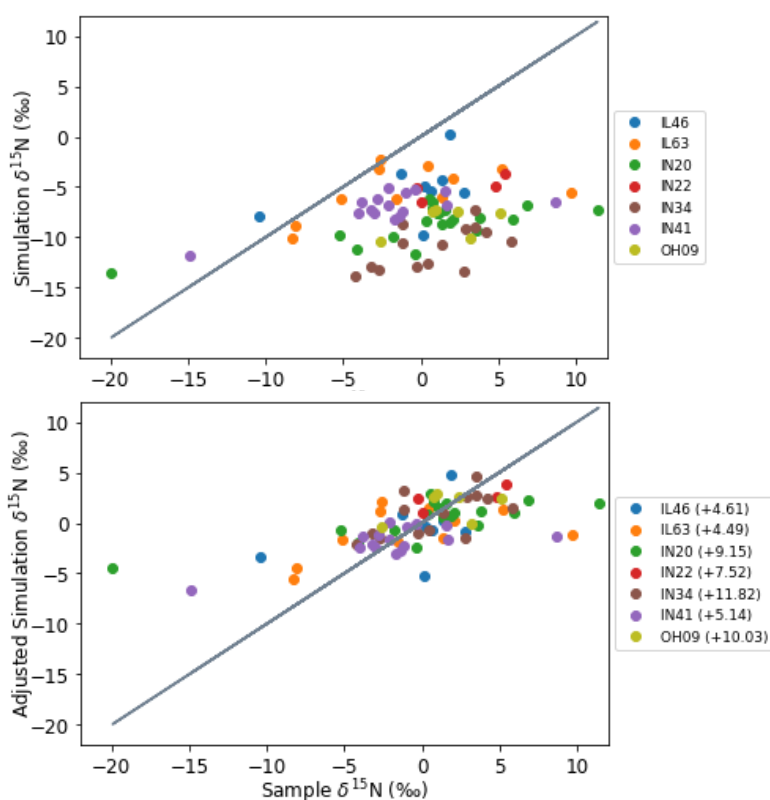
Figure 14: The emission + transport + enhanced NO_x loss CMAQ predicted $\delta^{15}N$ value of NO_x deposition using NEI-2002 and 2002 meteorology compared to the measured $\delta^{15}N$ of rain NO_3^- at NADP sites within IN, IL, and OH. The photochemical isotope enrichment factor (‰) correction used for each site is noted in the legend.

NADP site. After adjusting the simulated δ^{15}N by raising the values by the average of the difference between sample δ^{15}N and simulated δ^{15}N for each site, the scatter plots of sample δ^{15}N vs. simulated δ^{15}N well fit into the one-to-one line (Fig. 14, bottom). The complete ^{15}N incorporated chemical mechanisms will be explored in future study.

4. Conclusion

The evolution of δ^{15}N values along the "journey" of atmospheric NO_x were traced, using our ^{15}N incorporated SMOKE and CMAQ. The $\delta^{15}NO_x$ under the "emission only" scenario was simulated by SMOKE, using the NO_x emissions from NEI emission sectors and the corresponding δ^{15}N values from previous research. The SMOKE simulation indicates that the NO_x emission from biogenic sources is the key driver for the variation of δ^{15}N, especially among the Midwestern NADP sites. The uncertainties in the $\delta^{15}NO_x$ emission are less than 5‰ over the majority of the grids within the Midwest, which were well below the difference among the assigned $\delta^{15}NO_x$ values for different NO_x emission sources (Fig. S24). The $\delta^{15}NO_x$ under the "emission + transport" scenario was simulated by CMAQ, using the ^{15}N incorporated emission input dataset generated from SMOKE, as well as the meteorology input dataset generated from WRF and MCIP. The CMAQ simulation indicates that the PBL height is the key driver for the mixture of anthropogenic and natural NO_x emission, which deepens the gap between δ^{15}N of atmospheric NO_x and NO_x emission. The $\delta^{15}NO_x$ under the "emission + transport + enhanced NO_x loss" scenario was simulated by enhancing NO_x deposition in CMAQ simulation, to show how "lifetime chemistry" alters $\delta^{15}NO_x$ values before it can be transported along significant distances, assuming no isotope fractionation during chemical conversion or deposition.

The simulations under "emission only" scenario and "emission + transport + enhanced NO_x loss" scenario were compared to the measurements in West Lafayette, Indiana. The simulated δ^{15}N agreed well with the seasonal trend and monthly variation. The simulated $\delta^{15}NO_x$ under the "emission only" scenario was less negative than the corresponding measurements in West Lafayette, IN, taken from July to August 2016. Thus, if we only consider the effects from NO_x emission sources, the emission from soil, livestock waste, off-road vehicles, and natural gas power plant in West Lafayette, IN are possible to be underestimated, and the emission from the on-road vehicle and coal-fired power plant in West Lafayette, IN are possibly overestimated. The simulated $\delta^{15}NO_x$ under the "emission + transport + enhanced NO_x loss" scenario was about 3‰ closer to the corresponding measurements in West Lafayette, IN, comparing to the "emission only" simulations. The simulations under "emission + transport + enhanced NO_x loss" scenario was also compared to the measurements of $\delta^{15}NO_3^-$ from NADP sites within Indiana, Illinois, Ohio, and Kentucky. The sample-by-sample comparison shows a moderate positive correlation between observed and simulated $\delta^{15}NO_3^-$, with negative bias varies among the NADP sites. This bias is attributed to isotope fractionation during the conversion NO_x into NO_y, affected by different NO_x, VOC, and oxidant loading, as well as temperature, and photolysis rate at each NADP site. Therefore, the future work is to explore how tropospheric photochemistry alters $\delta^{15}NO_x$ by incorporating ^{15}N into the chemical mechanism of CMAQ and comparing the simulation with the corresponding measurements. With the validation of our nitrogen isotopes incorporated CMAQ, the NO_x emission inventories could be effectively evaluated and improved.

Data availability: The source code for SMOKE version 4.6 is available at https://github.com/CEMPD/SMOKE/releases/tag/SMOKEv46_Sep2018. The source code for CMAQ version 5.2.1 is available at https://github.com/USEPA/CMAQ/tree/5.2.1. The in-detail simulation results for $\delta^{15}N$ of NO_x emission based on 2002 and 2016 versions of National Emission Inventory and the associated python codes are achieved on Zenodo.org (10.5281/zenodo.4048992). The input datasets for WRF simulation are available at https://www.ncei.noaa.gov/data/. The in-detail simulation results for $\delta^{15}N$ of atmospheric NO_x under all scenarios discussed in this paper and the CMAQ-based c-shell script for generating BCON for extracted domain simulation are achieved on Zenodo.org (10.5281/zenodo.4311986).

Author contributions: Huan Fang and Greg Michalski were the investigator for the project and organized the tasks. Huan Fang develop the model codes, performed the simulation to incorporate ^{15}N into SMOKE outputs and generated $\delta^{15}N$ values and reconstruct CMAQ by incorporating ^{15}N, and performed the simulation to generate $\delta^{15}N$ values. Greg Michalski helped Huan Fang in interpreting the results. Huan Fang prepared the manuscript with contributions from all co-authors.

Acknowledgments: We would like to thank the Purdue Research Foundation, the Purdue Climate Change Research Center, and the National Science Foundation (AGS award 1903646) for providing funding for the project. We would like to thank Scott Spak from School of Urban & Regional Planning, University of Iowa for simulating SMOKE using NEI-2002. We would like to thank Tomas Ratkus from Department of Earth, Atmospheric, and Planetary Sciences, Steven Plite, and Frank Bakhit from Rosen Center for Advanced Computing, Purdue University for setting up CMAQ on Purdue research computing for this project.

References:

Almaraz, M., Bai, E., Wang, C., Trousdell, J., Conley, S., Faloona, I. and Houlton, B. Z.: Agriculture is a major source of NOx pollution in California, Sci. Adv., doi:10.1126/sciadv.aao3477, 2018.

Ammann, M., Siegwolf, R., Pichlmayer, F., Suter, M., Saurer, M. and Brunold, C.: Estimating the uptake of traffic-derived NO2 from 15N abundance in Norway spruce needles, Oecologia, doi:10.1007/s004420050710, 1999.

Beirle, S., Spichtinger, N., Stohl, A., Cummins, K. L., Turner, T., Boccippio, D., Cooper, O. R., Wenig, M., Grzegorski, M., Platt, U. and Wagner, T.: Estimating the NOx produced by lightning from GOME and NLDN data: A case study in the Gulf of Mexico, Atmos. Chem. Phys., doi:10.5194/acp-6-1075-2006, 2006.

Boersma, K. F., Eskes, H. J., Meijer, E. W. and Kelder, H. M.: Estimates of lightning NOx; production from GOME satellite observations, Atmos. Chem. Phys., doi:10.5194/acp-5-2311-2005, 2005.

Bradshaw, J., Davis, D., Grodzinsky, G., Smyth, S., Newell, R., Sandholm, S. and Liu, S.: Observed distributions of nitrogen oxides in the remote free troposphere from the NASA Global Tropospheric Experiment programs, Rev. Geophys., doi:10.1029/1999RG900015, 2000.

Byun, D., Pleim, J., Tang, R. and Bourgeois, A.: Meteorology-Chemistry Interface Processor (MCIP) for Models-3 Community Multiscale Air Quality (CMAQ) Modeling System, System, 1999.

Chameides, W. L., Davis, D. D., Bradshaw, J., Rodgers, M., Sandholm, S. and Bai, D. B.: An estimate of the NO x production rate in electrified clouds based on NO observations from the GTE/CITE 1 fall 1983 field operation , J. Geophys. Res., doi:10.1029/jd092id02p02153, 1987.

Chang, Y., Zhang, Y., Tian, C., Zhang, S., Ma, X., Cao, F., Liu, X., Zhang, W., Kuhn, T. and Lehmann, M. F.: Nitrogen isotope fractionation during gas-to-particle conversion of NOx to NO3- in the atmosphere - Implications for isotope-based NO x source apportionment, Atmos. Chem. Phys., doi:10.5194/acp-18-11647-2018, 2018.

Christian, H. J., Blakeslee, R. J., Boccippio, D. J., Boeck, W. L., Buechler, D. E., Driscoll, K. T., Goodman, S. J., Hall, J. M., Koshak, W. J., Mach, D. M. and Stewart, M. F.: Global frequency and distribution of lightning as observed from space by the Optical Transient Detector, J. Geophys. Res. Atmos., doi:10.1029/2002jd002347, 2003.

Cicero-Fernândez, P., Long, J. R. and Winer, A. M.: Effects of Grades and Other Loads on On-Road Emissions of Hydrocarbons and Carbon Monoxide, J. Air Waste Manag. Assoc., doi:10.1080/10473289.1997.10464455, 1997.

Dameris, M., Grewe, V., Ponater, M., Deckert, R., Eyring, V., Mager, F., Matthes, S., Schnadt, C., Stenke, A., Steil, B., Brühl, C. and Giorgetta, M. A.: Long-term changes and variability in a

transient simulation with a chemistry-climate model employing realistic forcing, Atmos. Chem. Phys., doi:10.5194/acp-5-2121-2005, 2005.

Davidson, E. A.: Pulses of nitric oxide and nitrous oxide flux following wetting of dry soil: an assessment of probable sources and importance relative to annual fluxes, Trace gas Exch. a Glob. Perspect., 1992.

Davidson, E. A. and Kingerlee, W.: A global inventory of nitric oxide emissions from soils, Nutr. Cycl. Agroecosystems, doi:10.1023/a:1009738715891, 1997.

de Foy, B., Lu, Z., Streets, D. G., Lamsal, L. N. and Duncan, B. N.: Estimates of power plant NOx emissions and lifetimes from OMI NO2 satellite retrievals, Atmos. Environ., doi:10.1016/j.atmosenv.2015.05.056, 2015.

De Laeter, J. R., Böhlke, J. K., De Bièvre, P., Hidaka, H., Peiser, H. S., Rosman, K. J. R. and Taylor, P. D. P.: Atomic weights of the elements: Review 2000 (IUPAC Technical Report), Pure Appl. Chem., doi:10.1351/pac200375060683, 2003.

DeCaria, A. J., Pickering, K. E., Stenchikov, G. L. and Ott, L. E.: Lightning-generated NOx and its impact on tropospheric ozone production: A three-dimensional modeling study of a Stratosphere-Troposphere Experiment: Radiation, Aerosols and Ozone (STERAO-A) thunderstorm, J. Geophys. Res. D Atmos., doi:10.1029/2004JD005556, 2005.

Dentener, F. J. and Crutzen, P. J.: Reaction of N2O5 on tropospheric aerosols: impact on the global distributions of NOx, O3, and OH, J. Geophys. Res., doi:10.1029/92JD02979, 1993.

Dignon, J. and Hameed, S.: Global emissions of nitrogen and sulfur oxides from 1860 to 1980, J. Air Waste Manag. Assoc., doi:10.1080/08940630.1989.10466519, 1989.

Dreher, D. B. and Harley, R. A.: A fuel-based inventory for heavy-duty diesel truck emissions, J. Air Waste Manag. Assoc., doi:10.1080/10473289.1998.10463686, 1998.

Duncan, B. N., Yoshida, Y., De Foy, B., Lamsal, L. N., Streets, D. G., Lu, Z., Pickering, K. E. and Krotkov, N. A.: The observed response of Ozone Monitoring Instrument (OMI) NO2 columns to NOx emission controls on power plants in the United States: 2005-2011, Atmos. Environ., doi:10.1016/j.atmosenv.2013.08.068, 2013.

Elliott, E. M., Kendall, C., Boyer, E. W., Burns, D. A., Lear, G. G., Golden, H. E., Harlin, K., Bytnerowicz, A., Butler, T. J. and Glatz, R.: Dual nitrate isotopes in dry deposition: Utility for partitioning NO x source contributions to landscape nitrogen deposition, J. Geophys. Res. Biogeosciences, doi:10.1029/2008JG000889, 2009.

Elliott, E. M., Kendall, C., Wankel, S. D., Burns, D. A., Boyer, E. W., Harlin, K., Bain, D. J. and Butler, T. J.: Nitrogen isotopes as indicators of NOx source contributions to atmospheric nitrate deposition across the midwestern and northeastern United States, Environ. Sci. Technol., doi:10.1021/es070898t, 2007.

Farrell, A., Carter, R. and Raufer, R.: The NOx Budget: Market-based control of tropospheric ozone in the northeastern United States, Resour. Energy Econ., doi:10.1016/S0928-7655(98)00035-9, 1999.

Fehr, T., Höller, H. and Huntreiser, H.: Model study on production and transport of lightning-produced NOx in a EULINOX supercell storm, J. Geophys. Res. D Atmos., doi:10.1029/2003JD003935, 2004.

Felix, J. D., Elliott, E. M. and Shaw, S. L.: Nitrogen isotopic composition of coal-fired power plant NOx: Influence of emission controls and implications for global emission inventories, Environ. Sci. Technol., doi:10.1021/es203355v, 2012.

Felix, J. D. and Elliott, E. M.: The agricultural history of human-nitrogen interactions as recorded in ice core $\delta15N-NO3-$, Geophys. Res. Lett., doi:10.1002/grl.50209, 2013.

Felix, J. D. and Elliott, E. M.: Isotopic composition of passively collected nitrogen dioxide emissions: Vehicle, soil and livestock source signatures, Atmos. Environ., doi:10.1016/j.atmosenv.2014.04.005, 2014.

Felix, J. D., Elliott, E. M., Avery, G. B., Kieber, R. J., Mead, R. N., Willey, J. D. and Mullaugh, K. M.: Isotopic composition of nitrate in sequential Hurricane Irene precipitation samples: Implications for changing NOx sources, Atmos. Environ., doi:10.1016/j.atmosenv.2015.01.075, 2015.

Fang, H., Walters, W. W., Mase, D., and Michalski, G.: i_NRACM: incorporating ^{15}N into the Regional Atmospheric Chemistry Mechanism (RACM) for assessing the role photochemistry plays in controlling the isotopic composition of NO_x, NO_y, and atmospheric nitrate, Geosci. Model Dev., 14, 5001–5022, https://doi.org/10.5194/gmd-14-5001-2021, 2021.

Fibiger, D. L., Hastings, M. G., Lew, A. F. and Peltier, R. E.: Collection of NO and NO2 for isotopic analysis of NOx emissions, Anal. Chem., doi:10.1021/ac502968e, 2014.

Fraser, A., Goutail, F., McLinden, C. A., Melo, S. M. L. and Strong, K.: Lightning-produced NO2 observed by two ground-based UV-visible spectrometers at Vanscoy, Saskatchewan in August 2004, Atmos. Chem. Phys., doi:10.5194/acp-7-1683-2007, 2007.

Fujita, E. M., Croes, B. E., Bennett, C. L., Lawson, D. R., Lurmann, F. W. and Main, H. H.: Comparison of emission inventory and ambient concentration ratios of CO, NMOG, and NOx in California's South Coast Air Basin, J. Air Waste Manag. Assoc., doi:10.1080/10473289.1992.10466989, 1992.

Fujita, E. M., Campbell, D. E., Zielinska, B. B., Sagebiel, J. C., Bowen, J. L., Goliff, W. S., Stockwell, W. R. and Lawson, D. R.: Diurnal and weekday variations in the source contributions of ozone precursors in California's South Coast Air Basin, J. Air Waste Manag. Assoc., doi:10.1080/10473289.2003.10466226, 2003.

Fujita, E. M., Stockwell, W. R., Campbell, D. E., Keislar, R. E. and Lawson, D. R.: Evolution of the magnitude and spatial extent of the weekend ozone effect in California's South Coast Air Basin, 1981–2000, J. Air Waste Manag. Assoc., doi:10.1080/10473289.2003.10466225, 2003.

Galbally, I. E. and Roy, C. R.: Loss of fixed nitrogen from soils by nitric oxide exhalation, Nature, doi:10.1038/275734a0, 1978

Gallardo, L. and Rodhe, H.: Oxidized nitrogen in the remote Pacific: The role of electrical discharges over the oceans, J. Atmos. Chem., doi:10.1023/A:1005738402496, 1997.

Galloway, J. N. and Cowling, E. B.: Reactive nitrogen and the world: 200 Years of change, in Ambio., 2002.

Galloway, J. N., Dentener, F. J., Capone, D. G., Boyer, E. W., Howarth, R. W., Seitzinger, S. P., Asner, G. P., Cleveland, C. C., Green, P. A., Holland, E. A., Karl, D. M., Michaels, A. F., Porter, J. H., Townsend, A. R. and Vörösmarty, C. J.: Nitrogen cycles: Past, present, and future, Biogeochemistry, doi:10.1007/s10533-004-0370-0, 2004.

Ganzeveld, L. N., Lelieveld, J., Dentener, F. J., Krol, M. C., Bouwman, A. J. and Roelofs, G. J.: Global soil-biogenic NOX emissions and the role of canopy processes, J. Geophys. Res. Atmos., doi:10.1029/2001JD001289, 2002.

Garten, C. T.: Nitrogen isotope composition of ammonium and nitrate in bulk precipitation and forest throughfall, Int. J. Environ. Anal. Chem., doi:10.1080/03067319208027017, 1992.

Gauss, M., Myhre, G., Isaksen, I. S. A., Grewe, V., Pitari, G., Wild, O., Collins, W. J., Dentener, F. J., Ellingsen, K., Gohar, L. K., Hauglustaine, D. A., Iachetti, D., Lamarque, J. F., Mancini, E., Mickley, L. J., Prather, M. J., Pyle, J. A., Sanderson, M. G., Shine, K. P., Stevenson, D. S., Sudo, K., Szopa, S. and Zeng, G.: Radiative forcing since preindustrial times due to ozone change in the troposphere and the lower stratosphere, Atmos. Chem. Phys., doi:10.5194/acp-6-575-2006, 2006.

Grell, G. A., Dudhia, J., & Stauffer, D. R.: A description of the fifth-generation Penn State/NCAR mesoscale model (MM5), NCAR Technical Note NCAR/TN-398+ STR, 1994.

Hall, S. J., Ogata, E. M., Weintraub, S. R., Baker, M. A., Ehleringer, J. R., Czimczik, C. I. and Bowling, D. R.: Convergence in nitrogen deposition and cryptic isotopic variation across urban and agricultural valleys in northern Utah, J. Geophys. Res. Biogeosciences, doi:10.1002/2016JG003354, 2016.

Hanson, P. J. and Lindberg, S. E.: Dry deposition of reactive nitrogen compounds: A review of leaf, canopy and non-foliar measurements, Atmos. Environ. Part A, Gen. Top., doi:10.1016/0960-1686(91)90020-8, 1991.

Harley, R. A., McKeen, S. A., Pearson, J., Rodgers, M. O. and Lonneman, W. A.: Analysis of motor vehicle emissions during the Nashville/Middle Tennessee Ozone Study, J. Geophys. Res. Atmos., doi:10.1029/2000JD900677, 2001.

Heaton, T. H. E.: 15N14N ratios of nitrate and ammonium in rain at Pretoria, South Africa, Atmos. Environ., doi:10.1016/0004-6981(87)90080-1, 1987.

Heaton, T. H. E.: 15N/14N ratios of NOx from vehicle engines and coal-fired power stations, Tellus B, doi:10.1034/j.1600-0889.1990.00007.x-i1, 1990.

Hoering, T.: The isotopic composition of the ammonia and the nitrate ion in rain, Geochim. Cosmochim. Acta, doi:10.1016/0016-7037(57)90021-2, 1957.

Houlton, B. Z., Boyer, E., Finzi, A., Galloway, J., Leach, A., Liptzin, D., Melillo, J., Rosenstock, T. S., Sobota, D. and Townsend, A. R.: Intentional versus unintentional nitrogen use in the United States: Trends, efficiency and implications, Biogeochemistry, doi:10.1007/s10533-012-9801-5, 2013.

Houyoux, M.: Clean Air Interstate Rule Emissions Inventory Technical Support Document. US EPA, 2005.

Hudman, R. C., Moore, N. E., Mebust, A. K., Martin, R. V., Russell, A. R., Valin, L. C. and Cohen, R. C.: Steps towards a mechanistic model of global soil nitric oxide emissions: Implementation and space based-constraints, Atmos. Chem. Phys., doi:10.5194/acp-12-7779-2012, 2012.

Huntrieser, H., Schlager, H., Feigl, C. and Höller, H.: Transport and production of NOX in electrified thunderstorms: Survey of previous studies and new observations at midlatitudes, J. Geophys. Res. Atmos., doi:10.1029/98JD02353, 1998.

Huntrieser, H., Feigl, C., Schlager, H., Schröder, F., Gerbig, C., van Velthoven, P., Flatøy, F., Théry, C., Petzold, A., Höller, H. and Schumann, U.: Airborne measurements of NOx, tracer species, and small particles during the European lightning nitrogen oxides experiment, J. Geophys. Res. Atmos., doi:10.1029/2000jd000209, 2002.

Ingalls, M. N.: On-road vehicle emission factors from measurements in a Los Angeles area tunnel, in Proceedings - A&WMA Annual Meeting., 1989.

Jacob, D. J. and Wofsy, S. C.: Budgets of reactive nitrogen, hydrocarbons, and ozone over the Amazon forest during the wet season, J. Geophys. Res., doi:10.1029/jd095id10p16737, 1990.

Jaeglé, L., Steinberger, L., Martin, R. V. and Chance, K.: Global partitioning of NOx sources using satellite observations: Relative roles of fossil fuel combustion, biomass burning and soil emissions, in Faraday Discussions., 2005.

Johansson, C.: Pine forest: a negligible sink for atmospheric NO x in rural Sweden , Tellus B Chem. Phys. Meteorol., doi:10.3402/tellusb.v39i5.15360, 1987.

Kim, S. W., Heckel, A., Frost, G. J., Richter, A., Gleason, J., Burrows, J. P., McKeen, S., Hsie, E. Y., Granier, C. and Trainer, M.: NO2 columns in the western United States observed from space and simulated by a regional chemistry model and their implications for NO x emissions, J. Geophys. Res. Atmos., doi:10.1029/2008JD011343, 2009.

Koike, M., Kondo, Y., Kita, K., Takegawa, N., Nishi, N., Kashihara, T., Kawakami, S., Kudoh, S., Blake, D., Shirai, T., Liley, B., Ko, M. K., Miyazaki, Y., Kawasaki, Z. and Ogawa, T.: Measurements of reactive nitrogen produced by tropical thunderstorms during BIBLE-C, J. Geophys. Res. Atmos., doi:10.1029/2006JD008193, 2007.

Laughner, J. L., & Cohen, R. C.: Direct observation of changing NOx lifetime in North American cities, Science, 366(6466), 723-727, 2019.

Lawrence, M. G., Chameides, W. L., Kasibhatla, P. S., Levy, H. and Moxim, W.: Lightning and atmospheric chemistry: The rate of atmospheric NO production, in Handbook of Atmospheric Electrodynamics., 2017.

Lerdau, M. T., Munger, J. W. and Jacob, D. J.: The NO2 flux conundrum, Science (80-.)., doi:10.1126/science.289.5488.2291, 2000.

Levy, H., Moxim, W. J. and Kasibhatla, P. S.: A global three-dimensional time-dependent lightning source of tropospheric NOx, J. Geophys. Res. Atmos., doi:10.1029/96jd02341, 1996.

Li, D. and Wang, X.: Nitrogen isotopic signature of soil-released nitric oxide (NO) after fertilizer application, Atmos. Environ., doi:10.1016/j.atmosenv.2008.01.042, 2008.

Li, Y., Schichtel, B. A., Walker, J. T., Schwede, D. B., Chen, X., Lehmann, C. M. B., Puchalski, M. A., Gay, D. A. and Collett, J. L.: Increasing importance of deposition of reduced nitrogen in the United States, Proc. Natl. Acad. Sci. U. S. A., doi:10.1073/pnas.1525736113, 2016.

Liao, T., Gui, K., Jiang, W., Wang, S., Wang, B., Zeng, Z., Che, H., Wang, Y. and Sun, Y.: Air stagnation and its impact on air quality during winter in Sichuan and Chongqing, southwestern China, Sci. Total Environ., doi:10.1016/j.scitotenv.2018.04.122, 2018.

Lighty, J. A. S., Veranth, J. M. and Sarofim, A. F.: Combustion aerosols: Factors governing their size and composition and implications to human health, J. Air Waste Manag. Assoc., doi:10.1080/10473289.2000.10464197, 2000.

Liu, L., Guo, J., Miao, Y., Liu, L., Li, J., Chen, D., He, J. and Cui, C.: Elucidating the relationship between aerosol concentration and summertime boundary layer structure in central China, Environ. Pollut., doi:10.1016/j.envpol.2018.06.008, 2018.

Lu, Z., Streets, D. G., De Foy, B., Lamsal, L. N., Duncan, B. N. and Xing, J.: Emissions of nitrogen oxides from US urban areas: Estimation from Ozone Monitoring Instrument retrievals for 2005-2014, Atmos. Chem. Phys., doi:10.5194/acp-15-10367-2015, 2015.

Ludwig, J., Meixner, F. X., Vogel, B. and Forstner, J.: Soil-air exchange of nitric oxide: An overview of processes, environmental factors, and modeling studies, Biogeochemistry, doi:10.1023/A:1006424330555, 2001.

Martin, R. V., Sauvage, B., Folkins, I., Sioris, C. E., Booone, C., Bernath, P. and Ziemke, J.: Space-based constraints on the production of nitric oxide by lightning, J. Geophys. Res. Atmos., doi:10.1029/2006JD007831, 2007.

Mase, D. F.: A coupled modeling and observational approach to understanding oxygen-18 in atmospheric nitrate, Ph. D. thesis, Purdue University, United States of America, 2010.

McDonald, B. C., McKeen, S. A., Cui, Y. Y., Ahmadov, R., Kim, S. W., Frost, G. J., ... & Trainer, M.: Modeling ozone in the eastern US using a fuel-based mobile source emissions inventory, Environmental science & technology, 52(13), 7360-7370, 2018.

Miao, Y., Guo, J., Liu, S., Zhao, C., Li, X., Zhang, G., Wei, W. and Ma, Y.: Impacts of synoptic condition and planetary boundary layer structure on the trans-boundary aerosol transport from Beijing-Tianjin-Hebei region to northeast China, Atmos. Environ., doi:10.1016/j.atmosenv.2018.03.005, 2018.

Miao, Y., Li, J., Miao, S., Che, H., Wang, Y., Zhang, X., Zhu, R. and Liu, S.: Interaction Between Planetary Boundary Layer and PM2.5 Pollution in Megacities in China: a Review, Curr. Pollut. Reports, doi:10.1007/s40726-019-00124-5, 2019.

Miller, D. J., Wojtal, P. K., Clark, S. C. and Hastings, M. G.: Vehicle NOx emission plume isotopic signatures: Spatial variability across the eastern United States, J. Geophys. Res., doi:10.1002/2016JD025877, 2017.

Miller, D. J., Chai, J., Guo, F., Dell, C. J., Karsten, H. and Hastings, M. G.: Isotopic Composition of In Situ Soil NOx Emissions in Manure-Fertilized Cropland, Geophys. Res. Lett., doi:10.1029/2018GL079619, 2018.

Miyazaki, K., Eskes, H. J., & Sudo, K.: Global NO x emission estimates derived from an assimilation of OMI tropospheric NO 2 columns, Atmospheric Chemistry and Physics, 12(5), 2263-2288, 2012.

Moore, H.: The isotopic composition of ammonia, nitrogen dioxide and nitrate in the atmosphere, Atmos. Environ., doi:10.1016/0004-6981(77)90102-0, 1977.

Muller, J. F.: Geographical distribution and seasonal variation of surface emissions and deposition velocities of atmospheric trace gases, J. Geophys. Res., doi:10.1029/91JD02757, 1992.

Müller, J.-F. and Stavrakou, T.: Inversion of CO and NOx emissions using the adjoint of the IMAGES model, Atmos. Chem. Phys., doi:10.5194/acp-5-1157-2005, 2005.

Murray, L. T.: Lightning NOx and Impacts on Air Quality, Curr. Pollut. Reports, doi:10.1007/s40726-016-0031-7, 2016.

National Centers for Environmental Information: U.S. Wind Climatology, Available from: https://www.ncdc.noaa.gov/societal-impacts/wind/, 2019.

National Centers for Environmental Information: Model Datasets, available from: https://www.ncdc.noaa.gov/data-access/model-data/model-datasets, 2019.

Occhipinti, C., Aneja, V. P., Showers, W. and Niyogi, D.: Back-trajectory analysis and source-receptor relationships: Particulate matter and nitrogen isotopic composition in rainwater, Journal of the Air and Waste Management Association., 2008.

Oke, T. R.: Boundary Layer Climates., 2002.

Ott, L. E., Pickering, K. E., Stenchikov, G. L., Huntrieser, H. and Schumann, U.: Effects of lightning NOx production during the 21 July European Lightning Nitrogen Oxides Project storm studied with a three-dimensional cloud-scale chemical transport model, J. Geophys. Res. Atmos., doi:10.1029/2006JD007365, 2007.

Parrish, D. D.: Critical evaluation of US on-road vehicle emission inventories, Atmos. Environ., doi:10.1016/j.atmosenv.2005.11.033, 2006.

Pearson, J., Wells, D. M., Seller, K. J., Bennett, A., Soares, A., Woodall, J. and Ingrouille, M. J.: Traffic exposure increases natural 15N and heavy metal concentrations in mosses, New Phytol., doi:10.1046/j.1469-8137.2000.00702.x, 2000.

Pierce, T. E.: Reconsideration of the Emission Factors assumed in BEIS3 for Three USGS Vegetation Categories: Shrubland, Coniferous Forest, and Deciduous Forest, 2001.

Pierson, W. R., Gertler, A. W. and Bradow, R. L.: Comparison of the scaqs tunnel study with other onroad vehicle emission data, J. Air Waste Manag. Assoc., doi:10.1080/10473289.1990.10466799, 1990.

Pierson, W. R., Gertler, A. W., Robinson, N. F., Sagebiel, J. C., Zielinska, B., Bishop, G. A., Stedman, D. H., Zweidinger, R. B. and Ray, W. D.: Real-world automotive emissions - summary of studies in the Fort McHenry and Tuscarora Mountain Tunnels, in Atmospheric Environment., 1996.

Pilegaard, K.: Processes regulating nitric oxide emissions from soils, Philos. Trans. R. Soc. B Biol. Sci., doi:10.1098/rstb.2013.0126, 2013.

Potter, C. S., Matson, P. A., Vitousek, P. M. and Davidson, E. A.: Process modeling of controls on nitrogen trace gas emissions from soils worldwide, J. Geophys. Res. Atmos., doi:10.1029/95JD02028, 1996.

Pouliot, G., & Pierce, T. E.: Integration of the Model of Emissions of Gases and Aerosols from Nature (MEGAN) into the CMAQ Modeling System, in: 18th International Emission Inventory Conference, Baltimore, Maryland, 14 April 2009, 14-17, 2009.

Rasool, Q. Z., Zhang, R., Lash, B., Cohan, D. S., Cooter, E. J., Bash, J. O., & Lamsal, L. N.: Enhanced representation of soil NO emissions in the Community Multiscale Air Quality (CMAQ) model version 5.0. 2, Geoscientific Model Development, 9(9), 3177-3197, 2016

Redling, K., Elliott, E., Bain, D. and Sherwell, J.: Highway contributions to reactive nitrogen deposition: Tracing the fate of vehicular NOx using stable isotopes and plant biomonitors, Biogeochemistry, doi:10.1007/s10533-013-9857-x, 2013.

Ridley, B. A., Dye, J. E., Walega, J. G., Zheng, J., Grahek, F. E. and Rison, W.: On the production of active nitrogen by thunderstorms over New Mexico, J. Geophys. Res. Atmos., doi:10.1029/96jd01706, 1996.

Ridley, B., Ott, L., Pickering, K., Emmons, L., Montzka, D., Weinheimer, A., Knapp, D., Grahek, F., Li, L., Heymsfield, G., McGill, M., Kucera, P., Mahoney, M. J., Baumgardner, D., Schultz, M. and Brasseur, G.: Florida thunderstorms: A faucet of reactive nitrogen to the upper troposphere, J. Geophys. Res. D Atmos., doi:10.1029/2004JD004769, 2004.

Riha, K. M.: The use of stable isotopes to constrain the nitrogen cycle, Ph. D. thesis, Purdue University, United States of America, 2013.

Russell, K. M., Galloway, J. N., MacKo, S. A., Moody, J. L. and Scudlark, J. R.: Sources of nitrogen in wet deposition to the Chesapeake Bay region, Atmos. Environ., doi:10.1016/S1352-2310(98)00044-2, 1998.

Savard, M. M., Bégin, C., Smirnoff, A., Marion, J. and Rioux-Paquette, E.: Tree-ring nitrogen isotopes reflect anthropogenic NOx emissions and climatic effects, Environ. Sci. Technol., doi:10.1021/es802437k, 2009.

Savard, M. M., Cole, A., Smirnoff, A. and Vet, R.: Δ15N values of atmospheric N species simultaneously collected using sector-based samplers distant from sources – Isotopic inheritance and fractionation, Atmos. Environ., doi:10.1016/j.atmosenv.2017.05.010, 2017.

Sawyer, R. F., Harley, R. A., Cadle, S. H., Norbeck, J. M., Slott, R. and Bravo, H. A.: Mobile sources critical review: 1998 NARSTO assessment, Atmos. Environ., doi:10.1016/S1352-2310(99)00463-X, 2000.

Scholes, M. C., Martin, R., Scholes, R. J., Parsons, D. and Winstead, E.: NO and N2O emissions from savanna soils following the first simulated rains of the season, Nutr. Cycl. Agroecosystems, doi:10.1023/a:1009781420199, 1997.

Schumann, U., Kurz, C., Schlager, H., Huntrieser, H., Emmons, L., Labrador, L., Meijer, E., Ulanovsky, A. and Viciani, S.: Towards a robust estimate of the global lightning nitrogen oxides source rate and its error bound, in European Space Agency, (Special Publication) ESA SP., 2006.

Schumann, U. and Huntrieser, H.: The global lightning-induced nitrogen oxides source, Atmos. Chem. Phys., doi:10.5194/acp-7-3823-2007, 2007.

Schwartz, S. E.: The Whitehouse effect - Shortwave radiative forcing of climate by anthropogenic aerosols: An overview, J. Aerosol Sci., doi:10.1016/0021-8502(95)00533-1, 1996.

Schwede, D., Pouliot, G. and Pierce, T.: Changes to the biogenic emissions inventory system version 3 (BEIS3), in 4th Annual CMAS User's Conference., 2005.

Selden, T. M., Forrest, A. S., & Lockhart, J. E.: Analyzing the reductions in US air pollution emissions: 1970 to 1990, Land Economics, 1-21, doi: 10.2307/3146990, 1999.

Shepherd, M. F., Barzetti, S. and Hastie, D. R.: The production of atmospheric NOx and N2O from a fertilized agricultural soil, Atmos. Environ. Part A, Gen. Top., doi:10.1016/0960-1686(91)90277-E, 1991.

Shu, L., Xie, M., Gao, D., Wang, T., Fang, D., Liu, Q., Huang, A. and Peng, L.: Regional severe particle pollution and its association with synoptic weather patterns in the Yangtze River Delta region, China, Atmos. Chem. Phys., doi:10.5194/acp-17-12871-2017, 2017.

Singer, B. C. and Harley, R. A.: A Fuel-Based Motor Vehicle Emission Inventory, J. Air Waste Manag. Assoc., doi:10.1080/10473289.1996.10467492, 1996.

Singer, B. C. and Harley, R. A.: A fuel-based inventory of motor vehicle exhaust emissions in the Los Angeles area during summer 1997, Atmos. Environ., doi:10.1016/S1352-2310(99)00358-1, 2000.

Skamarock, W. C., Dye, J. E., Defer, E., Barth, M. C., Stith, J. L., Ridley, B. A. and Baumann, K.: Observational- and modeling-based budget of lightning-produced NOx in a continental thunderstorm, J. Geophys. Res. Atmos., doi:10.1029/2002jd002163, 2003.

Slovik, S., Siegmund, A., Fuhrer, H. W. and Heber, U.: Stomatal uptake of SO2, NOx and O3 by spruce crowns (Picea abies) and canopy damage in Central Europe, New Phytol., doi:10.1111/j.1469-8137.1996.tb01884.x, 1996.

Snape, C. E., Sun, C., Fallick, A. E., Irons, R. and Haskell, J.: Potential of stable nitrogen isotope ratio measurements to resolve fuel and thermal NOx in coal combustion, Fuel Chem. Div. Prepr., 2003.

Snyder, J. P.: Map projections - a working manual, US Geol. Surv. Prof. Pap., 1987.

Song, W., Liu, X. Y., Hu, C. C., Chen, G. Y., Liu, X. J., Walters, W. W., ... & Liu, C. Q.: Important contributions of non-fossil fuel nitrogen oxides emissions, Nature communications, 12(1), 1-7, 2021

Spak, S., Holloway, T., Mednick, A., & Stone, B.: Evaluation of Bottom-Up Mobile Emissions Inventories in the Upper Midwest, in: American Geophysical Union Fall Meeting, San Francisco, California, 10-14 Dec 2007, 2007.

Srivastava, R. K., Neuffer, W., Grano, D., Khan, S., Staudt, J. E. and Jozewicz, W.: Controlling NO x emission from industrial sources, Environ. Prog., doi:10.1002/ep.10063, 2005.

Staudt, A. C., Jacob, D. J., Ravetta, F., Logan, J. A., Bachiochi, D., Sandholm, S., Ridley, B., Singh, H. B. and Talbot, B.: Sources and chemistry of nitrogen oxides over the tropical Pacific, J. Geophys. Res. Atmos., doi:10.1029/2002jd002139, 2003.

Stavrakou, T., Müller, J. F., Boersma, K. F., Van Der A., R. J., Kurokawa, J., Ohara, T. and Zhang, Q.: Key chemical NOx sink uncertainties and how they influence top-down emissions of nitrogen oxides, Atmos. Chem. Phys., doi:10.5194/acp-13-9057-2013, 2013.

Stehfest, E. and Bouwman, L.: N2O and NO emission from agricultural fields and soils under natural vegetation: Summarizing available measurement data and modeling of global annual emissions, Nutr. Cycl. Agroecosystems, doi:10.1007/s10705-006-9000-7, 2006.

Stevenson, D. S., Dentener, F. J., Schultz, M. G., Ellingsen, K., van Noije, T. P. C., Wild, O., Zeng, G., Amann, M., Atherton, C. S., Bell, N., Bergmann, D. J., Bey, I., Butler, T., Cofala, J., Collins, W. J., Derwent, R. G., Doherty, R. M., Drevet, J., Eskes, H. J., Fiore, A. M., Gauss, M., Hauglustaine, D. A., Horowitz, L. W., Isaksen, I. S. A., Krol, M. C., Lamarque, J. F., Lawrence, M. G., Montanaro, V., Müller, J. F., Pitari, G., Prather, M. J., Pyle, J. A., Rast, S., Rodriquez, J. M., Sanderson, M. G., Savage, N. H., Shindell, D. T., Strahan, S. E., Sudo, K. and Szopa, S.: Multimodel ensemble simulations of present-day and near-future tropospheric ozone, J. Geophys. Res. Atmos., doi:10.1029/2005JD006338, 2006.

The Institute for the Environment - The University of North Carolina at Chapel Hill: SMOKE v4.5 User's Manual, Available from: https://www.cmascenter.org/smoke/documentation/4.5/html/, 2017.

Thoene, B., Rennenberg, H. and Weber, P.: Absorption of atmospheric NO2 by spruce (Picea abies) trees: II. Parameterization of NO2 fluxes by controlled dynamic chamber experiments, New Phytol., doi:10.1111/j.1469-8137.1996.tb04630.x, 1996.

Thomas, R. J., Krehbiel, P. R., Rison, W., Hamlin, T., Boccippio, D. J., Goodman, S. J. and Christian, H. J.: Comparison of ground-based 3-dimensional lightning mapping observations

with satellite-based LIS observations in Oklahoma, Geophys. Res. Lett., doi:10.1029/1999GL010845, 2000.

Tie, X., Zhang, R., Brasseur, G. and Lei, W.: Global NOx production by lightning, J. Atmos. Chem., doi:10.1023/A:1016145719608, 2002.

Tost, H., Jöckel, P. and Lelieveld, J.: Lightning and convection parameterisations - Uncertainties in global modelling, Atmos. Chem. Phys., doi:10.5194/acp-7-4553-2007, 2007.

United States Census Bureau: 2007−2011 American Community Survey 5-Year Estimates, travel time to work by zip code, table B08303, Available from: https://www.census.gov/programs-surveys/acs/technical-documentation/table-and-geography-changes/2011/5-year.html, 2019.

United States Energy Information Administration: Electricity, Available from: https://www.eia.gov/electricity/data/eia860/, 2017a.

United States Energy Information Administration: U.S. electric generating capacity increase in 2016 was largest net change since 2011, Available from: https://www.eia.gov/todayinenergy/detail.php?id=30112, 2017b.

United States Environmental Protection Agency: National Emissions Inventory (NEI), Available from: https://www.epa.gov/air-emissions-inventories/national-emissions-inventory-nei, 2014.

United States Environmental Protection Agency: Biogenic Emissions Landuse Database, Available from: https://www.epa.gov/air-emissions-modeling/biogenic-emissions-landuse-database-version-3-beld3, 2018a.

United States Environmental Protection Agency: 2002 National Emissions Inventory (NEI) Booklet, Available from: https://archive.epa.gov/epa/air-emissions-inventories/2002-national-emissions-inventory-nei-booklet.html, 2018b

US Environmental Protection Agency: User's Guide to MOBILE6.1 and MOBILE6.2 Mobile Source Emission Factor Model, Tech. Rep. EPA420-R-03-010, 2003.

Van Noije, T. P. C., Eskes, H. J., Dentener, F. J., Stevenson, D. S., Ellingsen, K., Schultz, M. G., Wild, O., Amann, M., Atherton, C. S., Bergmann, D. J., Bey, I., Boersma, K. F., Butler, T., Cofala, J., Drevet, J., Fiore, A. M., Gauss, M., Hauglustaine, D. A., Horowitz, L. W., Isaksen, I. S. A., Krol, M. C., Lamarque, J. F., Lawrence, M. G., Martin, R. V., Montanaro, V., Müller, J. F., Pitari, G., Prather, M. J., Pyle, J. A., Richter, A., Rodriguez, J. M., Savage, N. H., Strahan, S. E., Sudo, K., Szopa, S. and Van Roozendael, M.: Multi-model ensemble simulations of tropospheric NO2 compared with GOME retrievals for the year 2000, Atmos. Chem. Phys., doi:10.5194/acp-6-2943-2006, 2006.

Vinken, G. C. M., Boersma, K. F., Maasakkers, J. D., Adon, M., & Martin, R. V.: Worldwide biogenic soil NO x emissions inferred from OMI NO 2 observations, Atmospheric Chemistry and Physics, 14(18), 10363-10381, 2014

Vukovich, J., & Pierce, T.: The implementation of BEIS3 within the SMOKE modeling framework, in: Proceedings of the 11th International Emissions Inventory Conference, Atlanta, Georgia, 15 April 2002, 15-18, 2002.

Walters, W. W., Goodwin, S. R. and Michalski, G.: Nitrogen stable isotope composition ($\delta^{15}N$) of vehicle-emitted NOx, Environ. Sci. Technol., doi:10.1021/es505580v, 2015a.

Walters, W. W., Tharp, B. D., Fang, H., Kozak, B. J. and Michalski, G.: Nitrogen Isotope Composition of Thermally Produced NOx from Various Fossil-Fuel Combustion Sources, Environ. Sci. Technol., doi:10.1021/acs.est.5b02769, 2015b.

Walters, W. W. and Michalski, G.: Theoretical calculation of nitrogen isotope equilibrium exchange fractionation factors for various NOy molecules, Geochim. Cosmochim. Acta, doi:10.1016/j.gca.2015.05.029, 2015.

Walters, W. W., Simonini, D. S. and Michalski, G.: Nitrogen isotope exchange between NO and NO2 and its implications for δ15N variations in tropospheric NOx and atmospheric nitrate, Geophys. Res. Lett., doi:10.1002/2015GL066438, 2016.

Walters, W. W., Fang, H. and Michalski, G.: Summertime diurnal variations in the isotopic composition of atmospheric nitrogen dioxide at a small midwestern United States city, Atmos. Environ., doi:10.1016/j.atmosenv.2018.01.047, 2018.

Weber, P. and Rennenberg, H.: Dependency of nitrogen dioxide (NO2) fluxes to wheat (Triticum aestivum L.) leaves from NO2 concentration, light intensity, temperature and relative humidity determined from controlled dynamic chamber experiments, Atmos. Environ., doi:10.1016/1352-2310(96)00008-8, 1996.

Wong, S., Wang, W. C., Isaksen, I. S. A., Berntsen, T. K. and Sundet, J. K.: A global climate-chemistry model study of present-day tropospheric chemistry and radiative forcing from changes in tropospheric O3 since the preindustrial period, J. Geophys. Res. D Atmos., doi:10.1029/2003JD003998, 2004.

Xing, J., Pleim, J., Mathur, R., Pouliot, G., Hogrefe, C., Gan, C. M. and Wei, C.: Historical gaseous and primary aerosol emissions in the United States from 1990 to 2010, Atmos. Chem. Phys., doi:10.5194/acp-13-7531-2013, 2013.

Yan, X., Ohara, T. and Akimoto, H.: Statistical modeling of global soil NOX emissions, Global Biogeochem. Cycles, doi:10.1029/2004GB002276, 2005.

Yienger, J. J. and Levy, H.: Empirical model of global soil-biogenic NOx emissions, J. Geophys. Res., doi:10.1029/95jd00370, 1995.

Yu, Z. and Elliott, E. M.: Novel Method for Nitrogen Isotopic Analysis of Soil-Emitted Nitric Oxide, Environ. Sci. Technol., doi:10.1021/acs.est.7b00592, 2017.

2 Zörner, J., Penning de Vries, M. J. M., Beirle, S., Sihler, H., Veres, P. R., Williams, J. and
3 Wagner, T.: Multi-satellite sensor study on precipitation-induced emission pulses of NO_x from
4 soils in semi-arid ecosystems, Atmos. Chem. Phys. Discuss., doi:10.5194/acp-2016-93, 2016.